SeqCup-Free: Sequential and Combinatorial Geometry-Free Identification of Unstable Points for Geodetic Deformation Monitoring

Vinicius Rofatto, Ivandro Klein, Marcelo Tomio Matsuoka, Paulo de Oliveira Camargo, Mauricio Roberto Veronez, Luiz Gonzaga Jr, Lincon Rodrigues Silva

https://doi.org/10.1590/SciELOPreprints.11415

Submitted on: 2025-03-04
Posted on: 2025-03-10 (version 1)
(YYYY-MM-DD)

SeqCup-Free: Sequential and Combinatorial Geometry-Free Identification of Unstable Points for Geodetic Deformation Monitoring

Vinicius Francisco Rofatto[1*], Ivandro Klein[2†], Marcelo Tomio Matsuoka[1†], Paulo de Oliveira Camargo[3†], Mauricio Roberto Veronez[4†], Luiz Gonzaga da Silveira da Silveira Jr.[4†], Lincon Rodrigues Silva[1†]

[1*]Institute of Geography, Geosciences and Health Collective, Federal University of Uberlândia, LMG Highway 746 KM 01, Monte Carmelo, 38500-000, MG, Brazil,https://orcid.org/0000-0003-1453-7530,https://orcid.org/0000-0002-2630-522X,https://orcid.org/0009-0000-5951-4434.
[2]Academic Department of Civil Construction, Federal Institute of Santa Catarina (IFSC), 950 Mauro Ramos Avenue - Downtown, Florianópolis, 88010-400, SC, Brazil,https://orcid.org/0000-0003-4296-592X.
[3]Department of Cartography, Faculty of Science and Technology (Presidente Prudente Campus) - UNESP, 305 Roberto Símonsen Street - Educational Center, Presidente Prudente, 19060-900, SP, Brazil,https://orcid.org/0000-0001-7648-1291.
[4]PPGCA / VIZLAB, University of Vale do Rio dos Sinos (UNISINOS), 950 Unisinos Avenue, Cristo Rei Neighborhood, São Leopoldo do Sul, 93022-750, RS, Brazil,https://orcid.org/0000-0002-5914-3546,https://orcid.org/0000-0002-7661-2447.

*Corresponding author(s). E-mail(s): vfrofatto@gmail.com;
Contributing authors: ivandroklein@gmail.com; tomiomatsuoka@gmail.com; paulo.camargo@unesp.br; VERONEZ@unisinos.br; lgonzagajr@gmail.com; silvarlincon201@gmail.com;
†These authors contributed equally to this work.

Abstract

Congruence analysis is widely used to monitor structural stability through statistical analysis of differences in estimated coordinates of geodetic network points across observation epochs. Traditional methods for the identification of unstable points rely on either iterative hypothesis tests or combinatorial procedures, each with inherent limitations. To overcome these, we propose the Sequential and Combinatorial Geometry-Free Unstable Point Identification (SeqCup-Free) method, which integrates combinatorial analysis and likelihood ratio tests within a sequential framework. Unlike conventional approaches, SeqCup-Free uses observation differences instead of estimated coordinates, which removes the need for geodetic network datum definition and maintains the statistical power of hypothesis tests. Additionally, we introduce a modified version, SeqCup-Mod, which extends the method to non-nested hypothesis tests and achieves high success rates. A critical aspect of our approach is the definition of the maximum number of points considered unstable, which avoids statistical overlap while allowing the system to detect the maximum possible displacements. Results from simulations and real geodetic network data show that SeqCup-Free provides consistent and, in some cases, superior performance compared to classical and recent methods in deformation monitoring.

Keywords: Quality Control, Reliability, Non-nested model, Hypothesis Testing

1 Introduction

One of today's major challenges in geodetic data analysis is to detect geometric changes in objects or regions that are subject to displacements and/or deformations, such as man-made structures like dams, dikes, bridges, wind turbines, or high towers, as well as natural Earth structures like volcanoes, mining areas, caves, or tectonic plates.

The analysis of monitoring measurement can be categorized into four deformation models: congruence model, kinematic model, static model, and dynamic model. The congruence model describes the deformations using displacement vectors without specifying the time and any factor related to the acting forces, and internal and external loads as well. The kinematic models describe the geometric changes in terms of temporal variations (velocities and accelerations), considering that the state of the object is permanently in motion, but also there are no concerns with the causes of the deformations. If there is interest in investigating the functional relationship between causative forces and geometrical reactions of the object, then the static model will be more suitable. In the latter, the deformations are described from the physical properties of the object (e.g., expansion coefficients, temperature, and lengths), so that the temporal aspects are not explicit in the model. Finally, the dynamic model combines static and kinematic models, i.e., deformations are linked to their influencing factors (causative forces, internal and external loads) and the object's physical properties (Welsch and Heunecke 2001). Due to its common usage, we restrict ourselves to

the congruence model which only tells us whether a part of an object (or the whole object) is deformed or not.

In congruence analysis, the investigated structure is typically monitored using a geodetic network, which is measured at least twice over time. These epochal measurements are then analyzed statistically. The geodetic network works as a displacement monitoring system. The statistical test is one of the most widely used approaches to the specification of deformation congruence models (Pelzer 1971; Mierlo 1978, 1979; Niemeier 1981; Caspary 2000; Heunecke et al. 2013; Nowel 2020). The robust approach is another one also widely used and has had important advances in recent years (Chen 1983; Duchnowski 2010, 2013; Nowel and Kamiński 2014; Zienkiewicz 2015; Zienkiewicz and Baryla 2015; Wiśniewski and Zienkiewicz 2016; Batilović et al. 2022); but it is not part of the scope of this work.

Typically, the input data is a vector composed of the differences between the coordinates of points estimated by least squares at an initial epoch (say, Epoch 1) and a current epoch (say, Epoch 2). The null hypothesis, denoted by $\mathcal{H}_0$, is formulated under the condition that all points are stable (points that have a congruent/rigid geometrical structure at both considered epochs). On the other hand, the alternative hypotheses are stipulated from the assumption that there is at least one unstable point. Since we do not know which point or group of points is unstable, a consecutive hypothesis test is often applied to identify one unstable point after the other (Lehmann and Lösler 2017). Such a test procedure is similar to the outlier screening by iterative data-snooping (Baarda 1968). However, the iterative consecutive hypothesis tests are non-rigorous because the alternative hypotheses are restricted to only one single unstable point. The point flagged as most suspected to be unstable in a given step is not inspected in the next iteration step. In addition, the result of a misidentification in a given iteration conditions the result of the next iteration Nowel (2020). The weakness of the iterative consecutive hypothesis tests for the case where multiple displacements are in play has been reported by some authors Hekimoglu et al. (2010, 2014); Durdag et al. (2018); Nowel (2020).

To overcome the problem of iterative procedures, a non-iterative combinatorial procedure emerges for the case where all possible combinations of displaced points are considered. Such a procedure consists of comparing all potential candidates for stable points at the same stage. Consequently, it is not necessary to consecutively point-by-point specify the congruence model. This method has been applied in some numerical examples and discussed in detail by Velsink (2015) and Velsink (2018).

Another interesting combinatorial method is discussed by Lehmann and Lösler (2017). They use various information criteria and select the model with the lowest information criterion value as the best among all candidate models. In this process, penalty terms are applied to address the issue of comparing models with different dimensions. The more points are modeled as unstable (higher dimension of the congruence model, i.e., a more complex model), the greater the chances of overfitting, as a model typically fits observations better with a larger number of parameters. Therefore, penalty terms are introduced to manage model complexity. As highlighted by Nowel (2020), the goodness of model fit combined with a penalty term constitutes an identification criterion. However, he cautions that there are many criteria, and it is

yet unclear which of these should be adopted. Furthermore, the computational load can also be a concern with the existing combinatorial methods.

Nowel (2020) used the possibilities of combinatorics and generalized likelihood ratio tests performed in iterative steps to overcome the weaknesses associated with both the iterative point-by-point model specification and the combinatorial-only method. The integration between the iterative and combinatorial procedures, to the best of the author's knowledge, was previously addressed in the work of (Klein et al. 2017), but in the context of identifying multiple simultaneous outliers. Although there has been substantial progress in this emerging field of combinatorics, there are still challenges that open up new research perspectives (Baselga 2011; Duchnowski 2010, 2013; Zienkiewicz and Baryla 2015; Zienkiewicz 2015; Wiśniewski and Zienkiewicz 2016; Biagi and Caldera 2013; Wujanz et al. 2018).

In this contribution, we present a method that integrates both combinatorial analysis and likelihood ratio tests in a sequential procedure, namely *Sequential and Combinatorial Geometry-Free Identification of Unstable Points for Deformation Monitoring* – SeqCup-Free. Here, we also applied a modified version of SeqCup (denoted by SeqCupMod), which is based on the principle of non-nested hypothesis testing, which dispenses with the verification of whether the null hypothesis is or is not a subset of the alternative hypothesis.

The SeqCup-Free method utilizes differences in observations from two epochs instead of estimated coordinates. The concept of using unadjusted (original) observation differences has been around for some time, as highlighted by Nowel and Kamiński (2014). Here, however, the vector of epoch-wise observation differences will represent the vector of '*errors*'. The first epoch of observations constitutes the initial state of the network and is therefore used as a reference in the displacement analysis. If there is no displacement of points after the first epoch of observations, the difference between the measurements of subsequent epochs and the first is expected to contain only the random fluctuations inherent to the measurement process. However, if there is a displacement of points after the first epoch of observations, biases should be introduced into the error vector to account for the changes in the position of points that occurred after the first epoch.

When adopting the differences of observations, we do not need to be concerned about the problem of defining the datum of the epochs and applications of the S-transformation (Baarda 1973; Aydin 2017; Nowel 2019; Erdogan et al. 2021). On the other hand, we must guarantee that the campaigns are always carried out with the same occupation of the points to be able to compare measurements between epochs – epoch-wise measurements.

The effect of the network geometry is also eliminated in our approach, such as in Hekimoglu et al. (2014). As a result, we do not need to be concerned about whether it is a linear model of a geodetic network (e.g., leveling or GNSS baseline networks) or non-linear (e.g., trilateration). As a benefit, we avoid the linearization which may reduce the detection power Lehmann and Lösler (2018).

Erdogan et al. (2021) presented a methodology for identifying unstable points based on analyzing the differences between measurements taken in two epochs, which they called the univariate approach. This approach has the benefit of reducing the

smearing and masking effect of displacements. Smearing means that one unstable point makes another stable point appear as unstable and masking means that one unstable point prevents another one from being identified. Unlike what we propose, the authors consider a model under the null hypothesis with one parameter being the mean of such differences, which, in a certain way, reduces the statistical power in detecting displacements. Furthermore, they do not control for false positive rates (Type I Error rate), also known as Probability of False Alarm ($\mathcal{P}_{FA}$), a term commonly used in literature dedicated to geodetic quality control (Teunissen 2018). This decision error refers to detecting displacement when there is none. This is because they generally consider that the test involves only a single alternative hypothesis, when in fact there are multiple tests, i.e., it involves multiple alternative hypotheses. Consequently, an approach that allows controlling the false alarms is needed. Here, we use a Monte Carlo method so that the user-defined probability of false alarms is efficiently controlled.

In addition, it is not yet clear how to choose the maximum number of points to be modeled as unstable (displaced), and this choice remains somewhat arbitrary. It is crucial to establish a stopping criterion based on the maximum number of points a network can identify as unstable, rather than relying solely on the non-rejection of the null hypothesis. Here, to avoid subjectivity, the maximum number of points to be inspected as displaced (unstable) is determined by computing the complement of the hat matrix, commonly known as the redundancy matrix (Prószyński and Kwaśniak 2018). This procedure avoids the problem of having non-separable models in identifying unstable points. Although identification can be done, it is important to let know that our sequential test is restricted to the redundancy of the network at hand.

This paper is organized as follows. Section 2 provides a detailed description of the SeqCup-Free method and its underlying principles. In the subsequent section, the mathematical framework behind the sequential and combinatorial approach of SeqCup-Free is developed, and we explain how the method eliminates the need for specifying a geodetic network datum. Additionally, we demonstrate how to construct the overall displacement-design matrix $\boldsymbol{C}$ with examples, particularly in the context of trilateration and leveling networks. We also introduce the redundancy-based approach for determining the maximum number of points to be inspected. In Section 4, we evaluate the performance of SeqCup-Free through simulations on trilateration networks, comparing its success rates with both classical and recent methods. In Section 5, we validate SeqCup-Free and its modified version (SeqCupMod) by comparing them against classical and contemporary methods based on specialized literature. Finally, Section 6 concludes with a summary of the main contributions and limitations of SeqCup-Free.

2 SeqCup-Free method and principles

For simplicity in the analysis, we consider only measurements that have passed quality control in each epoch (e.g., through an iterative data snooping procedure) and are thus free of outliers. Without loss of generality, the following discussion is restricted to two epochs.

Before we start our presentation of the proposed method, let's first keep in mind that in conventional deformation analysis (CDA), two epoch-wise estimated coordinates of identical geodetic network points—typically derived from least squares estimation (LSE)—are compared to identify unstable points. In this context, the vectors of estimated coordinates and their covariance matrices at both epochs must be referenced to a common datum, which can be achieved through the theory of the connection of two epoch adjustment results (Teunissen 1985).

Here, alternatively, we use the differences from two epoch-wise geodetic observations of identical quantities to determine whether a specific set of points across two epochs is stable/congruent or not. Thus, the SeqCup-Free procedure proceeds as follows.

2.1 Null and Alternative Hypotheses

To begin the presentation of the method, let us consider the example of two campaigns (two distinct epochs) of measurements performed on a geodetic network. We can stack the measurements into a vector of observations for each epoch, and with the support of the theory of errors, we can write the following equations:

$$\boldsymbol{y}^{(1)} = \boldsymbol{y_v} + \boldsymbol{e_v}^{(1)} \tag{1}$$

$$\boldsymbol{y}^{(2)} = \boldsymbol{y_v} + \boldsymbol{e_v}^{(2)} \tag{2}$$

with $\boldsymbol{y}^{(.)} \in \mathbb{R}^{n\times 1}$ the vectors of the observations, $\boldsymbol{y_v} \in \mathbb{R}^{n\times 1}$ the true, but unknown, vector of the observables, and $\boldsymbol{e_v}^{(.)} \in \mathbb{R}^{n\times 1}$ the unknown vectors of measurement errors (note: the indices '1' and '2' inside the curly braces represent the quantities related to the first and second epoch in time, respectively).

By subtracting the Epoch 2 (Eq. 2) from the Epoch 1 (Eq. 1), the vector of errors of the two-epoch geodetic observations differences is straightforwardly obtained from the measurement process, as follows:

$$\boldsymbol{\Delta y} = \boldsymbol{\Delta e_v} = \boldsymbol{e_v}^{(2)} - \boldsymbol{e_v}^{(1)} \tag{3}$$

with $\boldsymbol{\Delta y} \in \mathbb{R}^{n\times 1}$ the vector of the two-epoch geodetic observations differences and $\boldsymbol{\Delta e_v} \in \mathbb{R}^{n\times 1}$ the vector of errors from the two-epoch geodetic observations differences. It is important to highlight that the differences in the geodetic measurements are computed from the identical quantities (e.g., height differences, distances, directions, and/or GNSS baseline components) of each epoch in time. Note that the error vector in Eq.(3) arises directly from the experimental measurement process.

In displacement detection, the model under the null hypothesis, denoted by $\mathcal{H}_0$, is typically set up for the case where all points to be analyzed are treated as stable points. If $\mathcal{H}_0$ is true, only random errors are present in the error vector $\boldsymbol{\Delta e}$, and therefore, one would conclude that the network's geometry remained stable between the two observation periods. In that case, $\boldsymbol{\Delta e}$ in Eq.3 can be characterized as a normally distributed random vector with zero expectation, as follows:

$$\boldsymbol{\Delta e} \overset{\mathcal{H}_0}{\sim} N\left(\boldsymbol{0}, \boldsymbol{\Sigma_{\Delta e}}\right) \tag{4}$$

Thus, the null hypothesis $\mathcal{H}_0$ can be formulated as:

$$\mathcal{H}_0 : \mathbb{E}\{\boldsymbol{\Delta e}\} = \mathbf{0}, \quad \mathbb{D}\{\boldsymbol{\Delta e}\} = \boldsymbol{\Sigma}_{\boldsymbol{\Delta e}} = \boldsymbol{\Sigma}_{\boldsymbol{y}}^{(1)} + \boldsymbol{\Sigma}_{\boldsymbol{y}}^{(2)} \tag{5}$$

with $\mathbb{E}\{.\}$ the expectation operator, $\mathbb{D}\{.\}$ the dispersion operator, $\boldsymbol{\Sigma}_{\boldsymbol{\Delta e}}$ the given positive-definite variance matrix of $\boldsymbol{\Sigma}_{\boldsymbol{\Delta e}}$. The variance matrix $\boldsymbol{\Sigma}_{\boldsymbol{\Delta e}}$ was obtained by applying the law for the propagation of uncertainty to Eq.3, which results from summing the given variances matrices from Epoch 1 $\left(\boldsymbol{\Sigma}_{\boldsymbol{y}}^{(1)}\right)$, and Epoch 2, $\left(\boldsymbol{\Sigma}_{\boldsymbol{y}}^{(2)}\right)$. Note that $\boldsymbol{\Delta e}$ results from a parameter-free estimation under $\mathcal{H}_0$. From this point on, we denote it as $\boldsymbol{\Delta e_0}$ to indicate, when necessary, that it was obtained under $\mathcal{H}_0$.

If there were displacements of points after the first epoch of observations, the subsequent observations would no longer reflect the initial configuration of the geodetic network but rather a new configuration due to the point displacements. Consequently, $\mathcal{H}_0$ would no longer be valid.

The displacements introduce biases in the error vector, meaning that the error vector $\boldsymbol{\Delta e}$, which ideally would contain only probabilistic fluctuations inherent to the measurement process (such as in $\mathcal{H}_0$), is also systematically affected by the shifted points.

As the goal of the monitoring is to infer whether the network points are stable or not, we can test the null hypothesis $\mathcal{H}_0$ against possible alternative hypotheses. Here, the alternative hypotheses extend $\mathcal{H}_0$ by including an unknown displacement parameter vector $\boldsymbol{\nabla}^{q_j} \in \mathbb{R}^{q_j \times 1}$, which describes the disturbance in the measurements as a function of the displacement of a subset of q_j points, where j represents the dimension of the group of points to be inspected. The size of the group q can vary between $q_1 \leq q_j \leq q_{\max}$. The definition of the maximum number of points ($q_{\max}$) will be discussed in the next section.

Therefore, in general, the number of alternative hypotheses can be established according to the number of possible groups of points to be investigated, denoted by $K_{n_p}^{q_j}$. The generalized form of the alternative hypotheses can then be written as:

$$\mathcal{H}_{g_i}^{q_j} : \mathbb{E}\{\boldsymbol{\Delta e}\}_{g_i}^{q_j} = \boldsymbol{C}_{g_i}^{q_j} \boldsymbol{\nabla}_{g_i}^{q_j}, \quad \mathbb{D}\{\boldsymbol{\Delta e}\}_{g_i}^{q_j} = \boldsymbol{\Sigma}_{\boldsymbol{\Delta e}}, \quad i = 1, \ldots, K_{n_p}^{q_j}, \tag{6}$$

where

$$K_{n_p}^{q_j} = \binom{n_p}{q_j} = \frac{n_p!}{(n_p - q_j)!\, q_j!}. \tag{7}$$

In this context, $\boldsymbol{C} \in \mathbb{R}^{n \times q_j}$ is the matrix that captures the relationship between the potentially displaced points and the resulting changes in the measurements associated with these points (referred to as the displacement-design matrix); n_p represents the total number of points in the network; given that the dimension of the group is defined as q_j, there will be $i = 1, \ldots, K_{n_p}^{q_j}$ groups, and the index i corresponds to each specific group g_i.

The elements of the displacement-design matrix $\boldsymbol{C}$ consist exclusively of the values 0, +1, or -1. A value of +1 indicates that an i-th group g_i of q_j shifted points with magnitudes $\boldsymbol{\nabla}_{g_i}^{q_j}$ causes a positive distortion in the measurements connected to them,

-1 indicates a negative distortion, and 0 means that the points remained stable, with no distortion in the measurements between epochs.

A simple example of having only one single point as suspect to be displaced (i.e., q_1) is illustrated in the trilateration network in Fig.1. By considering that $g_1 = [A]$, $g_2 = [B]$, $g_3 = [C]$, $g_4 = [D]$, $g_5 = [E]$, $g_6 = [F]$, and by assuming that only point F moved to a new position, F', then the group to be analyzed would be $g_i = [F]$, $i = 6$. In that case, one would assume that only the observations connected to point F in the second epoch would undergo deformations (dashed red lines)—either stretching (+1) or compressing (-1)—relative to their initial states (Epoch 1). In contrast, the others would remain stable (0) (dashed blue lines). In this illustration (Fig.1), the shifted point F to its new position F' would cause the AF' segment gets smaller than its initial state AF. Consequently, the displacement of the F point of magnitude $\nabla_{g_6}^{q_1}$ would act with a negative sign (-1). The same would occur for BF; i.e., $\nabla_{g_6}^{q_1}$ would act with a negative sign (-1), which would cause BF' (Epoch 2) to be smaller than BF (Epoch 1); while the CF sign would be positive (+1) because the CF' (Epoch 2) segment becomes larger than CF (Epoch 1). The displacement-design matrix for that example would be described as a vector such that $\boldsymbol{C}_{g_6}^{q_1} = \begin{pmatrix} 0 & 0 & -1 & 0 & 0 & -1 & 0 & 0 & 1 \end{pmatrix}^\top$.

One of the key questions is how to define the number and locations of points to be monitored. Surveyors and geodesists must collaborate with other professionals to properly formulate an alternative model (Velsink 2018). Even with this information, uncertainties may persist about whether points initially considered stable might be shifting. From a practical standpoint, it is often unclear which points are stable or unstable. A more suitable approach is to apply a sequential test to determine the number and location of shifted points when the null model is rejected (Klein et al. 2017; Nowel 2020). In general, the core idea behind the proposed procedure is to identify the final congruence model by progressively increasing the number of deformation parameters.

2.2 Testing Procedure

The procedure begins by testing the null hypothesis $\mathcal{H}_0$ against a more conservative alternative hypothesis, which assumes that at least one point is moving among all points in the geodetic network. In this case, the alternative hypotheses are formulated according to Eq.(6) by setting $q_j = q_1$, such that

$$\mathcal{H}_{g_i}^{q_1} : \mathbb{E}\left\{\boldsymbol{\Delta e}\right\}_{g_i}^{q_1} = \boldsymbol{C}_{g_i}^{q_1} \nabla_{g_i}^{q_1}, \quad \mathbb{D}\left\{\boldsymbol{\Delta e}\right\}_{g_i}^{q_1} = \boldsymbol{\Sigma}_{\boldsymbol{\Delta e}}, \quad i = 1, \ldots, K_{n_p}^{q_1} \tag{8}$$

in which $g_i = [p_i]$ with $p_i \in \Omega$, where g_i represents the i-th group composed of only one single point p_i and $\Omega \in \mathbb{N}^{n_p}$ is the set of all n_p points in the network. For example, $g_1 = [1]$ denotes the first group with the point labeled '1', $g_2 = [2]$ denotes the second group with the point labeled '2', and so on. In this case, the number of alternative hypotheses is $K_{n_p}^{q_1} = \binom{n_p}{1} = n_p$. Note that the displacement-design matrix has been simplified to a vector $\boldsymbol{C}_{g_i}^{q_1} \in \mathbb{R}^{n \times 1}$ and the displacement parameter vector to a scalar $\nabla_{g_i}^{q_1} \in \mathbb{R}^{1 \times 1}$

This involves testing $\mathcal{H}_0$ against n_p alternative hypotheses. According to Eq.(4), the error vector under $\mathcal{H}_0$ is assumed to follow a multivariate normal distribution,

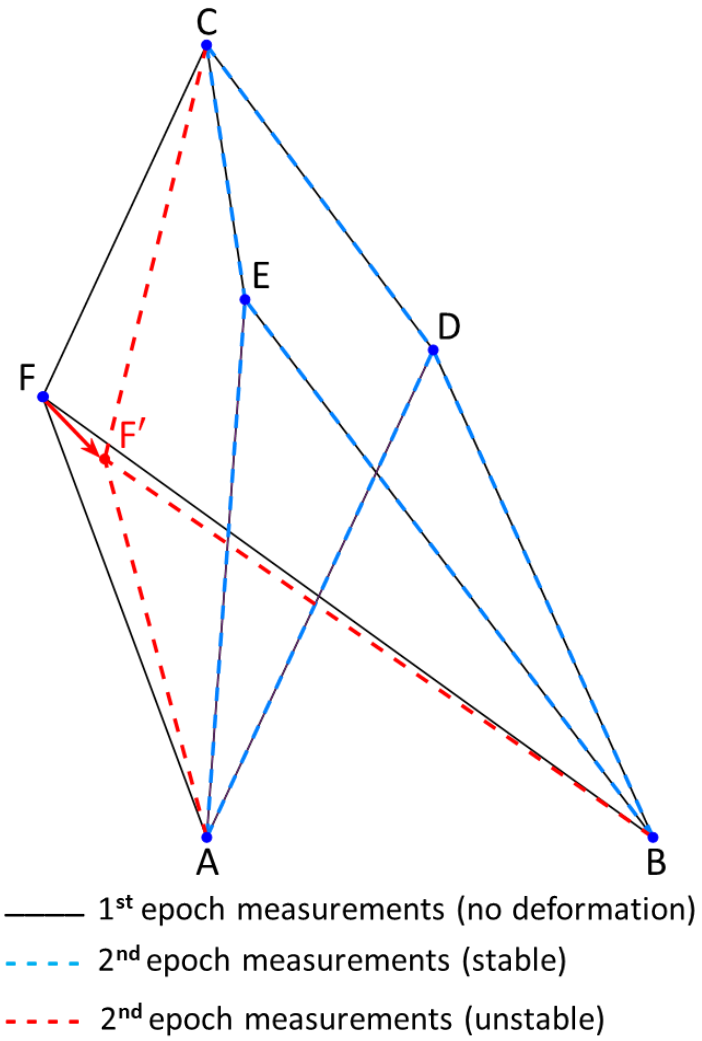

Fig. 1 Example of a horizontal trilateration network deformed due to the displacement (step) of point F to a new position F'.

while the error vectors under the alternative hypotheses $\left(\mathcal{H}_{g_i}^{q_1}\right)$ are given by:

$$\boldsymbol{\Delta e} \overset{\mathcal{H}_{g_i}^{q_1}}{\sim} N\left(\boldsymbol{C}_{g_i}^{q_1}\nabla_{g_i}^{q_1}, \boldsymbol{\Sigma}_{\boldsymbol{\Delta e}}\right), \quad \text{for } i = 1, \ldots, n_p \tag{9}$$

The reader can observe that under $\mathcal{H}_0$, the errors have means equal to zero, i.e., $\mathbb{E}\{\boldsymbol{\Delta e}\} = \mathbf{0}$, while under the alternative hypotheses $\mathcal{H}_A^{q_1}$, they have means of $\mathbb{E}\{\boldsymbol{\Delta e}\}_{g_i}^{q_1} = \boldsymbol{C}_{g_i}^{q_1}\nabla_{g_i}^{q_1}$, for $i = 1, \ldots, n_p$.

After postulating the null and alternative hypotheses, the test statistics derived from the concept of the generalized likelihood ratio test (GLRT) are then computed

as (e.g., Teunissen (2006)):

$$T_{g_i}^{q_1} = \underbrace{(\boldsymbol{\Delta e_0})^\top \boldsymbol{W} (\boldsymbol{\Delta e_0})}_{\mathcal{H}_0} - \underbrace{\left(\boldsymbol{\Delta}\hat{\boldsymbol{e}}_{g_i}^{q_1}\right)^\top \boldsymbol{W} \left(\boldsymbol{\Delta}\hat{\boldsymbol{e}}_{g_i}^{q_1}\right)}_{\mathcal{H}_A}, \quad i = 1, \ldots, n_p \tag{10}$$

in which the estimated error vectors under their corresponding alternative hypotheses $\boldsymbol{\Delta}\hat{\boldsymbol{e}}_{g_i}^{q_1} \in \mathbb{R}^{n\times 1}, i = 1, \ldots, n_p$ are given by:

$$\boldsymbol{\Delta}\hat{\boldsymbol{e}}_{g_i}^{q_1} = \boldsymbol{\Delta e} - \boldsymbol{C}_{g_i}^{q_1} \hat{\nabla}_{g_i}^{q_1}, \quad \text{for } i = 1, \ldots, n_p \tag{11}$$

with

$$\hat{\nabla}_{g_i}^{q_1} = \left[\left(\boldsymbol{C}_{g_i}^{q_1}\right)^\top \boldsymbol{W} \left(\boldsymbol{C}_{g_i}^{q_1}\right)\right]^{-1} \left(\boldsymbol{C}_{g_i}^{q_1}\right)^\top \boldsymbol{W}\, \boldsymbol{\Delta e}, \quad i = 1, \ldots, n_p \tag{12}$$

The known matrix of weights is defined as $\boldsymbol{W} = \boldsymbol{\Sigma}_{\boldsymbol{\Delta e}}^{-1}$ (Teunissen 2006; Klein et al. 2017). Details of the derivation of the GLRT in Eq. (10) can be found in Appendix A.

Now, we are interested in determining which of the alternative hypotheses may lead to the rejection of the null hypothesis with a certain probability. In this case, the test statistic of interest is the maximum test value, which is computed as

$$T_{max}^{q_1} = \max_{i \in 1,\ldots,n_p} T_{g_i}^{q_1} \tag{13}$$

The decision rule for this case is given by:

$$\text{Accept } \mathcal{H}_0 \text{ if } \; T_{max}^{q_1} \leq c_\alpha, \text{ reject otherwise in favour of } \mathcal{H}_{g_i}^{q_1}. \tag{14}$$

The decision rule in (14) states that if none of the n_p tests are rejected, the null hypothesis $\mathcal{H}_0$ is accepted. If $T_{max}^{q_1}$ exceeds a specific percentile of its probability distribution (i.e., a critical value), there is evidence that at least one point in the structure may be displaced. It is important to highlight that the maximum test statistic in Eq. (13) is treated directly as a test statistic. Thus, the critical value c_α is computed using the Monte Carlo method to control a user-defined Probability of False Alarm ($\mathcal{P}_{FA}$), denoted by α (Lehmann 2012). In the Appendix B, we provide details on how to compute the critical value c_α for the suggested procedure.

The rejection of $\mathcal{H}_0$ in (5) leads to the identification of the point most suspected to be displaced, i.e., the point that produced the maximum (extreme) test statistic $T_{max}^{q_1}$ that is larger than a critical value c_α. Therefore, point identification occurs only when detection is confirmed (i.e., $\mathcal{H}_0$ is rejected).

The model under the identified alternative hypothesis for q_1 then becomes the new null hypothesis: $\mathcal{H}_0 := \mathcal{H}_{g_i}^{q_1}$. In this case, the index j equals 1, which means that the new null hypothesis is given by the identified group g_i, whose dimension is one, $q_j = q_1$. For example, by assuming that a p-th point from the i-th group had been identified, $g_i = [p]$, the new null hypothesis would be written as $\mathcal{H}_0 := \mathcal{H}_{g_p}^{q_1}$.

The iterativeness of the procedure becomes evident as the model under the current null hypothesis, defined in the previous step for q_j, is now tested by assuming that a larger group of displaced points of dimension q_{j+1} may exist. The alternative

hypotheses are then formulated for all possible group combinations of q_{j+1} distinct points within the network, such that:

$$\mathcal{H}_{g_k}^{q_{j+1}} : \mathbb{E}\left\{\boldsymbol{\Delta e}\right\}_{g_k}^{q_{j+1}} = \boldsymbol{C}_{g_k}^{q_{j+1}} \boldsymbol{\nabla}_{g_k}^{q_{j+1}}, \quad \mathbb{D}\left\{\boldsymbol{\Delta \hat{e}}\right\}_{g_k}^{q_{j+1}} = \boldsymbol{\Sigma}_{\boldsymbol{\Delta e}}, \quad k = 1, \ldots, K_{n_p}^{q_{j+1}}, \quad (15)$$

Here, $g_k = [p_1, p_2, \ldots, p_{q_{j+1}}]$ represents the k-th group consisting of q_{j+1} different points, $p_1, p_2, \ldots, p_{q_{j+1}}$, from the set of all n_p points in the network Ω, with $k = 1, \ldots, K_{n_p}^{q_{j+1}}$. For example, for the previous case to be $q_j = q_1$, the new alternative hypotheses would be formulated for $q_{j+1} = q_2$.

The best model under the alternative hypotheses is then selected by computing the test statistics from Eq. (10) for q_{j+1} and identifying the corresponding candidate group by finding the maximum value of the test statistic from Eq. (13) for q_{j+1}, i.e., $T_{\max}^{q_{j+1}}$.

Hereafter, model selection involves applying a nested hypothesis test, where the null hypothesis is a subset of the alternative hypothesis. This means that the model under the null hypothesis must be contained within the model under the alternative hypothesis. In other words, the identified point group from the previous step, q_j, which became the current model under the null hypothesis, should be contained within the model of the current alternative hypothesis, which was formulated for an identified group of q_{j+1} points. This relationship implies that any parameter restrictions imposed by the null hypothesis are relaxed in the alternative hypothesis, which allows us to express it as:

$$\mathcal{H}_0 : \mathbb{E}\left\{\boldsymbol{\Delta e}\right\} = \boldsymbol{C}_{g_i}^{q_j} \boldsymbol{\nabla}_{g_i}^{q_j} \quad \text{against} \quad \mathcal{H}_A : \mathbb{E}\left\{\boldsymbol{\Delta e}\right\} = \boldsymbol{C}_{g_k}^{q_{j+1}} \boldsymbol{\nabla}_{g_k}^{q_{j+1}} \iff g_i \subseteq g_k \quad (16)$$

with g_i being the identified point group of smaller dimension for q_j and g_k the identified point group of larger dimension for q_{j+1}, so that g_i is contained within g_k.

If the condition described in Eq.(16) occurs, then the GLRT can be applied similarly to Eq.(10), but now for $\mathcal{H}_0 : \mathcal{H}_{g_i}^{q_j}$ against $\mathcal{H}_A : \mathcal{H}_{g_k}^{q_{j+1}}$, provided that $g_i \subseteq g_k$, as follows:

$$\Lambda_{\text{GLRT}} = \underbrace{\left(\boldsymbol{\Delta \hat{e}}_{g_i}^{q_j}\right)^\top \boldsymbol{W} \left(\boldsymbol{\Delta \hat{e}}_{g_i}^{q_j}\right)}_{\mathcal{H}_0} - \underbrace{\left(\boldsymbol{\Delta \hat{e}}_{g_k}^{q_{j+1}}\right)^\top \boldsymbol{W} \left(\boldsymbol{\Delta \hat{e}}_{g_k}^{q_{j+1}}\right)}_{\mathcal{H}_A} \iff g_i \subseteq g_k \quad (17)$$

The estimated error vectors $\left(\boldsymbol{\Delta \hat{e}}_{g_i}^{q_j}\right)$ and $\left(\boldsymbol{\Delta \hat{e}}_{g_k}^{q_{j+1}}\right)$ can be obtained by applying equations (11) and (12), according to the model dimension for q_j in $\mathcal{H}_0$ and q_{j+1} in $\mathcal{H}_A$. Thus, the selection of the best model is based on the following decision:

$$\text{Accept } \mathcal{H}_0 \text{ if } \Lambda_{\text{GLRT}} \leq c_\alpha; \text{ reject otherwise in favor of } \mathcal{H}_A. \quad (18)$$

If the null hypothesis is not rejected, the procedure ends, and only the point group identified in the previous step is flagged as unstable (e.g., a group g_i of dimension q_j in $\mathcal{H}_0$, as given by Eq. (16)). Otherwise, the procedure is repeated with the displacement model that considers the group of q_{j+1} points under the alternative hypothesis

as the new null hypothesis (e.g., $\mathcal{H}_0 := \mathcal{H}_{g_k}^{q_{j+1}}$). This new null hypothesis is then tested against alternative hypotheses formulated for displacement models of dimension q_{j+2}. The best model under the alternative hypothesis is selected based on the maximum value of the test statistic ($T_{\max}^{q_{j+2}}$), computed from Eq. (10) for all combinations of q_{j+2} distinct points in the entire network. Next, it is checked whether the point group flagged in the previous step, i.e., under the current null hypothesis (e.g., g_k of dimension q_{j+1}), is among those flagged in the current alternative hypothesis (e.g., g_l of dimension q_{j+2}). If this is the case, the GLRT is applied using Eq. (17) to decide between the null model defined by the group identified with dimension q_{j+1} and the alternative model with dimension q_{j+2}. This sequential procedure is repeated until one of the following conditions is met:

1. The current null hypothesis is not rejected.
2. More than one group of geodetic network points is identified by the extreme statistic $T_{\max}$ for a given q_j, which means the hypotheses are not separable (statistical overlap), and the identification cannot be accomplished.
3. The group of points identified in the previous step by $T_{\max}^{q_j}$ is not fully contained within the group identified by the current $T_{\max}^{q_{j+1}}$. If the null model is not a subset of the alternative model, the procedure ends by selecting the model under the null hypothesis defined by the group of points identified by $T_{\max}^{q_j}$.
4. The iteration reaches the threshold $q_{\max}$ (i.e., the maximum number of points to be evaluated is fully inspected).

In the next section, we will see that the maximum number of points to inspect depends on observation redundancy. Defining this limit also avoids equal maximum test statistics, preventing statistical overlap in identifying displaced points.

In general, therefore, the sequential testing procedure proposed here is based on the likelihood ratio, which we now call *Sequential and Combinatorial Geometry-Free Unstable Point identification* (SeqCup-Free). It consists of determining whether the additional subset of displaced points, considered in every new alternative hypothesis, is statistically significant or not, in terms of its impact on the quadratic form of the estimated observation errors, similar to its form for outlier detection (Klein et al. 2017). Consequently, we can identify the number and the location of the displaced geodetic network points. Fig.(2) provides step-by-step instructions on how to run the SeqCup-Free procedure.

2.3 Structure of C-Design Matrix

An overall displacement-design matrix $\boldsymbol{C}$ in expression 6 can be designed so that each column represents the displacement of a given point. The construction of the displacement-design matrix $\boldsymbol{C}$ depends on the type of network used.

Example for trilateration network: For instance, in a trilateration network that involves distance measurements, which are always positive, the design matrix is formed based on the sign of the difference between the distance measurements from two epochs. For this, we first provide an auxiliary matrix $\boldsymbol{A} \in \mathbb{R}^{n \times n_p}$ which describes the general case of the relationship between the measures (matrix rows) and the network points (matrix columns), but without taking into account the sign of the unknown

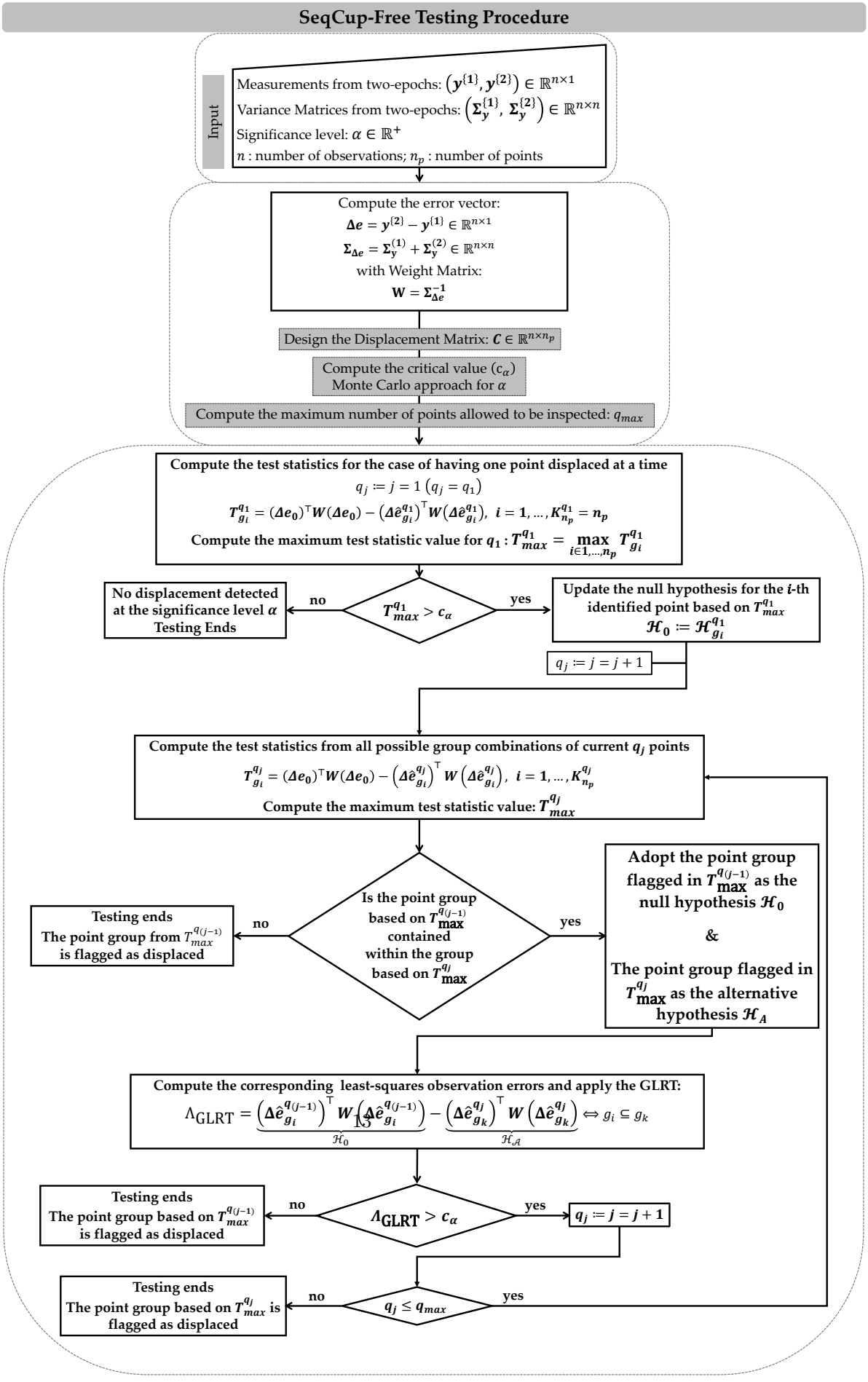

Fig. 2 Flowchart of the SeqCup-Free method.

estimable vector $\boldsymbol{\nabla}$. For instance, the auxiliary matrix $\boldsymbol{A}$ for the trilateration network in Fig.(1) is given by:

$$\boldsymbol{A} = \begin{pmatrix} \overbrace{1}^{A} & \overbrace{0}^{B} & \overbrace{0}^{C} & \overbrace{1}^{D} & \overbrace{0}^{E} & \overbrace{0}^{F} \\ 1 & 0 & 0 & 0 & 1 & 0 \\ 1 & 0 & 0 & 0 & 0 & 1 \\ 0 & 1 & 0 & 1 & 0 & 0 \\ 0 & 0 & 1 & 0 & 0 & 0 \\ 0 & 1 & 0 & 0 & 1 & 0 \\ 0 & 0 & 1 & 1 & 0 & 0 \\ 0 & 0 & 0 & 0 & 1 & 1 \\ 0 & 0 & 0 & 1 & 0 & 1 \end{pmatrix} \tag{19}$$

Then, the signs of the coefficients of the displacement-design matrix $\boldsymbol{C}$ can be obtained generically from the application of a *signum* function as:

$$\operatorname{sgn}\left[\Delta e_{(d)}\right] := \begin{cases} +1, & \text{if } \frac{\Delta e_{(d)}}{|\Delta e_{(d)}|} > 0, \\ -1, & \text{if } \frac{\Delta e_{(d)}}{|\Delta e_{(d)}|} < 0, \text{ for } d = 1, \ldots, n, \\ 0, & \text{if } \Delta e_{(d)} = 0. \end{cases} \tag{20}$$

where $sgn\,[.]$ is the sign function and $\left|\Delta e_{(d)}\right|$ gives a non-negativity value (absolute value) for each two-epoch geodetic observation differences. The result of Eq.(20) can be stacked into a *signum* vector as $\mathbf{s} \in \mathbb{R}^{n\times 1}$.Thus, the displacement-design matrix for the general case becomes:

$$\boldsymbol{C} = \operatorname{diag}(\mathbf{s})\,\boldsymbol{A} \tag{21}$$

where $\operatorname{diag}(.)$ is the diagonalization operator which converts a vector to a diagonal matrix.

Taking the example of the trilateration network in Fig. (1), and by considering that the error vector is given by
$\boldsymbol{\Delta e} = (-0.0019, 0.0013, 0.0027, 0.0027, -0.0029, 0.0071, -0.0054, 0.0010, -0.0103)^{\top}$, the *signum* vector would be given as $\boldsymbol{s} = (-1, 1, 1, 1, -1, 1, -1, 1, -1)^{\top}$. Thus, the displacement-design matrix $\boldsymbol{C}$ can be obtained from the Eq. (21) as follows:

$$\boldsymbol{C} = \begin{pmatrix} \overbrace{-1}^{A} & \overbrace{0}^{B} & \overbrace{0}^{C} & \overbrace{-1}^{D} & \overbrace{0}^{E} & \overbrace{0}^{F} \\ 1 & 0 & 0 & 0 & 1 & 0 \\ 1 & 0 & 0 & 0 & 0 & 1 \\ 0 & 1 & 0 & 1 & 0 & 0 \\ 0 & -1 & 0 & 0 & -1 & 0 \\ 0 & 1 & 0 & 0 & 0 & 1 \\ 0 & 0 & -1 & -1 & 0 & 0 \\ 0 & 0 & 1 & 0 & 1 & 0 \\ 0 & 0 & -1 & 0 & 0 & -1 \end{pmatrix} \tag{22}$$

Example for levelling network: The construction of the $\boldsymbol{C}$-matrix involves considerations about the nature of the type of observation of the geodetic network. In the

previous example, we demonstrate how to construct the $\boldsymbol{C}$-matrix for the case of trilateration networks (i.e., for the case in which we have distance measurements). In that case, distance is a quantity that naturally always manifests itself with a positive sign, independent of the direction of the line of sight. To properly model the displacement – i.e., whether the distance at epoch 2 has increased or decreased with respect to the reference epoch – a signal function is required for this type of network. However, this does not occur in the case where we have a levelling geodetic network. The signs of the height differences capture the sign of the displacement. As a simple example, consider a height difference measured from point i to point j in Epoch 1 ($\Delta h_{ij}^{(1)}$). The observation equation for this measurement, based on Eq. 1, is:

$$\Delta h_{ij}^{(1)} = [h_j - h_i]_v^{(1)} + e_{\Delta h_{ij}}^{(1)} \tag{23}$$

where $e_{\Delta h_{ij}}^{(1)}$ represents the random measurement error, and the subscript v indicates the true values of heights h_i and h_j.

One could imagine that a positive shift in the height of the point i, which was supposed, for example, to occur after the first epoch (say, Epoch 2) would be modeled as an extra (scalar) parameter (∇_{h_i}) as:

$$\Delta h_{ij}^{(2)} = [h_j - (h_i + \nabla_{h_i})]_v^{(2)} + e_{\Delta h_{ij}}^{(2)} \tag{24}$$

Consequently, the height difference observations between the two epochs would result in:

$$\Delta h_{ij}^{(2)} - \Delta h_{ij}^{(1)} = e_{\Delta h_{ij}}^{(2)} - e_{\Delta h_{ij}}^{(1)} - \nabla_{h_i} \tag{25}$$

In this example, the elevation of point i decreases the height difference between the points, and therefore, the element in the $\boldsymbol{C}$-matrix corresponding to the displacement of point i would be -1. Conversely, in the case of subsidence of point i, the height difference would increase ($+\nabla_{h_i}$). Therefore, the sign of the displacement ∇ comes directly from the relationship of the height difference.

An example of a leveling network of four points A, B, C, D is displayed in Fig.(3). In general, the full $\boldsymbol{C}$-matrix for that network would be given as:

$$\boldsymbol{C} = \begin{pmatrix} \overbrace{-1}^{A} & \overbrace{1}^{B} & \overbrace{0}^{C} & \overbrace{0}^{D} \\ -1 & 0 & 1 & 0 \\ 1 & 0 & 0 & -1 \\ 0 & -1 & 0 & 1 \\ 0 & -1 & 1 & 0 \\ 0 & 0 & -1 & 1 \end{pmatrix} \tag{26}$$

Important to highlight that the $\boldsymbol{C}$-matrix for the levelling networks follows the format of design matrix that is usually constructed for the case of estimating the unknown heights of the network.

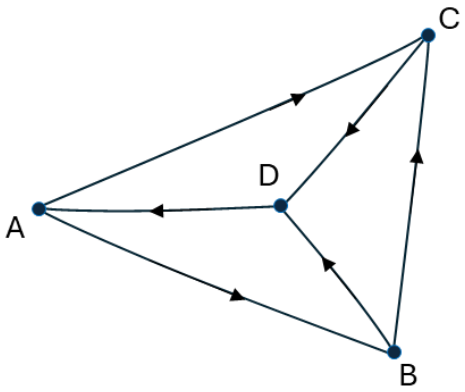

Fig. 3 Example of a Levelling Geodetic Network for Geodetic Monitoring Purposes.

2.4 Setting the maximum number of points to be inspected

Here, we demonstrate how to obtain the maximum dimension of the set of points $q_{\max}$ to be inspected by the SeqCup-Free procedure. The process of defining $q_{\max}$ involves identifying a model with sufficient redundancy to allow for the identification of unstable points.

If the maximum dimension $q_{\max}$ is defined as equal to the number of points in the network n_p, there will be a single maximum group $g_{\max}$ of n_p to be investigated. However, in this case, the matrix $\boldsymbol{C}$ will have a rank deficiency of one. This means that such a matrix cannot be considered invertible – it is then said to be singular. Consequently, it is not possible to compute the test statistics using Eq. 10. This demonstrates that the maximum dimension of the set of points must be at least $q_{\max} < n_p$.

By reducing the maximum number of points by one unit, i.e., $q_{\max} = \text{rank}(\boldsymbol{C}_{g_{\max}}^{q_{\max}}) = n_p - 1$, we now have a combination of $K_{n_p}^{n_p-1} = n_p$ groups of $n_p - 1$ points. All these groups will have full column rank. Otherwise, $q_{\max}$ should be reduced by one unit again to ensure regular models.

Next, the redundancy matrix, denoted by $\boldsymbol{R} \in \mathbb{R}^{n\times n}$, is computed for each of the n_p groups with a dimension of $q_{\max} = n_p - 1$. In its generic form, the redundancy matrix $\boldsymbol{R}$ is expressed as follows (see e.g., Teunissen (2006)):

$$\boldsymbol{R}_{g_i}^{q_{\max}} = \boldsymbol{I} - \boldsymbol{C}_{g_i}^{q_{\max}} \left(\boldsymbol{C}_{g_i}^{q_{\max}\top} \boldsymbol{W} \boldsymbol{C}_{g_i}^{q_{\max}} \right)^{-1} \boldsymbol{C}_{g_i}^{q_{\max}\top} \boldsymbol{W}, \quad i = 1, \ldots, n_p, \; q_{\max} = n_p - 1 \tag{27}$$

where $\boldsymbol{I} \in \mathbb{R}^{n\times n}$ is the identity matrix.

It can be verified that the estimated error, whether given by Eq. (11) or in its generalized form in Eq. (17), has a direct relationship with the redundancy matrix and can be written as (Lehmann 2012; Rofatto et al. 2020b):

$$\boldsymbol{\Delta}\hat{\boldsymbol{e}}_{g_i}^{q_{\max}} = \boldsymbol{R}_{g_i}^{q_{\max}} \boldsymbol{\Delta}\boldsymbol{e}, \quad i = 1, \ldots, K_{n_p}^{q_{\max}} \tag{28}$$

If the redundancy matrices for each group are equal, i.e., $\boldsymbol{R}_{g_1}^{q_{\max}} = \boldsymbol{R}_{g_2}^{q_{\max}} = \ldots = \boldsymbol{R}_{g_{n_p}}^{q_{\max}}$, then the test statistics derived from the GLRT, such as Eq. (10), will also be identical. This means that the models are not identifiable, and the value of the maximum test statistic will not return a single group, but all of them, resulting in a statistical overlap. In other words, it will not be possible to identify the alternative hypothesis, as the hypotheses will not be separable. In this case, $q_{\max}$ must be reduced again to ensure identifiability, so that the test statistics for each group are distinct from one another ($q_{\max} = n_p - 2$).

Next, the current redundancy matrices are computed for each group with a dimension defined by $q_{\max} = n_p - 2$. The number of groups will now be $K_{n_p}^{n_p-2}$. Generally, for $q_{\max} = n_p - 2$, the redundancy matrices will differ, and consequently, the test statistics will also be different. Even so, it is still necessary to verify whether the redundancy of each observation is sufficient to identify unstable points. To do this, the redundancy numbers, as a measure of the local internal reliability of the observations, must be analyzed.

The redundancy numbers (also known as local redundancy) are the diagonal elements of the matrix $\boldsymbol{R}$, denoted by r_{ll}, where $l = 1, \ldots, n$. As noted in Eq.(28), the larger the r_l, the greater the absorption of $\boldsymbol{\Delta}\hat{\boldsymbol{e}}$ in the vector of estimated errors $\boldsymbol{\Delta}\hat{\boldsymbol{e}}_{g_i}^{q_j}$, and therefore, the higher the power to detect unstable points. Prószyński and Kwaśniak (2018) recommends that redundancy numbers be greater than 0.5. Therefore, when calculating the redundancy matrix for each group of points, the smallest value of r_{ll} for each group must also be obtained $(\min r_{ll})_{g_i}^{q_{\max}}$, and it must be verified whether $\min\left(\min r_{ll}\right)_{g_i}^{q_{\max}} > 0.5$. If so, then $q_{\max}$ is defined (in our example, $q_{\max} = n_p - 2$). Otherwise, $q_{\max}$ must be reduced by one unit again (e.g., $q_{\max} = n_p - 3$), and the process repeated until the criterion $\min\left(\min r_{ll}\right)_{g_i}^{q_{\max}} > 0.5$ is satisfied. If $q_{\max} = 0$, we would have a situation where it is not possible to identify displacements, as the network lacks sufficient redundancy for this purpose. This situation may occur if the geodetic network is very poorly designed, making it impossible to identify displacements. This analysis can be extended to the problem of outlier identification. In general, the structure of the pseudo-code for determining $q_{\max}$ is given below:

1. Set $q_{\max} = n_p - 1$
2. Compute the redundancy matrix $\boldsymbol{R}_{g_i}^{q_{\max}}$ for each group.
3. Check if the redundancy matrices $\boldsymbol{R}_{g_1}^{q_{\max}} = \boldsymbol{R}_{g_2}^{q_{\max}} = \ldots = \boldsymbol{R}_{g_{n_p}}^{q_{\max}}$ are equal.
   - If they are equal, reduce $q_{\max}$ by 1 and return to item (2).
   - Otherwise, go to item (4).
4. Check $\min\left(\min r_{ll}\right)_{g_i}^{q_{\max}}$ for each group.
   - If $\min\left(\min r_{ll}\right)_{g_i}^{q_{\max}} > 0.5$, terminate the process and return $q_{\max}$ as the final value.
   - Otherwise, reduce $q_{\max}$ by 1 and return to item (2).
   - If $q_{\max} = 0$, terminate the process (insufficient redundancy).

Let's consider the example of the $\boldsymbol{C}$-matrix defined in (22) for the trilateration geodetic network displayed in Fig.(1). The observations are assumed to be

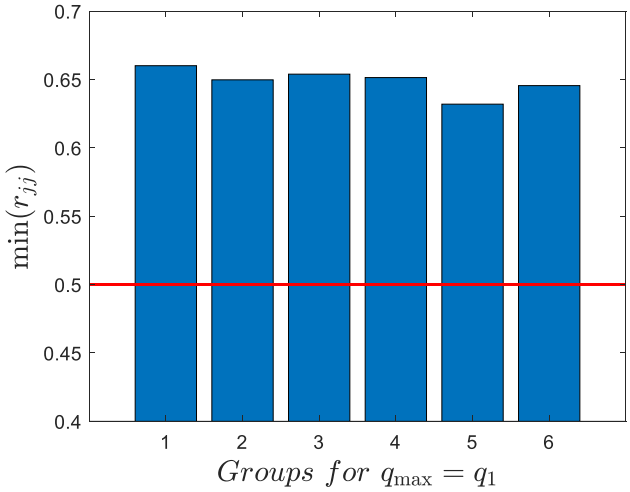

Fig. 4 Minimum redundancy numbers for q_1.

uncorrelated and with the same known variance of $\sigma^2 = 4\ mm^2$. In that case, the variance matrix for Epoch 2 is taken to be the same as in Epoch 1, so that $\boldsymbol{\Sigma_{\Delta e}} = \boldsymbol{\Sigma_y^{(1)}} + \boldsymbol{\Sigma_y^{(2)}} = 2\boldsymbol{\Sigma_y^{(1)}}$ and $\boldsymbol{W} = \boldsymbol{\Sigma_{\Delta e}^{-1}}$.

Note that for $q_{\max} = 6$, the full displacement-design matrix $\boldsymbol{C}$ is specified by taking the total number of points in the network, n_p, as shown in (22). It is easy to see that $rank(\boldsymbol{C}_{g_i}^{q_{\max}}) = 5$, which reveals a rank deficiency. The reader will notice that when setting $q_{\max} = n_p - 1 = q_5$, the redundancy matrices $\boldsymbol{R}_{g_1}^{q_5} = \boldsymbol{R}_{g_2}^{q_5} = \boldsymbol{R}_{g_3}^{q_5} = \boldsymbol{R}_{g_4}^{q_5} = \boldsymbol{R}_{g_5}^{q_5}$ are all equal. Thus, $q_{\max} = q_5$ is reduced by one unit, i.e., $q_{\max} = n_p - 2 = q_4$. However, since for $q_{\max} = q_4$, $\min\left(\min r_{ll}\right)_{g_i}^{q_4} \leq 0.5$, the maximum number of points to be simultaneously inspected is further reduced to $q_{\max} = n_p - 3 = q_3$. By repeating the process, we find that the $q_{\max}$ for this network would be $q_{\max} = q_1$, with $\min\left(\min r_{ll}\right)_{g_i}^{q_1} = 0.63 > 0.5$ (Figure 4).

A more flexible criterion for selecting $q_{\max}$ can also be proposed. Let us analyze the case where $q_{\max} = q_3$ and $q_{\max} = q_2$ for the same network before. Figure 5 shows the behavior of the minimum r_{ll} values when setting $q_{\max} = q_3$ and after reducing it to $q_{\max} = q_2$. It can be observed that for $q_{\max} = q_3$, most groups do not meet the criterion $r_{ll} > 0.5$ (yellow bars), whereas for $q_{\max} = q_2$, only five groups failed to meet the criterion, which the lowest redundancy numbers $\min(r_{ll})$ close to 0.5 (yellow bars).

Although our criterion is to evaluate the minimum of the lowest redundancy numbers, a less strict criterion could be, for instance, the average of the lowest redundancy numbers, as follows:

$$avg(\min r_{ll})_{g_i}^{q_{\max}} = \frac{\sum_{i=1}^{K_{n_p}^{q_{\max}}} (\min r_{ll})_{g_i}^{q_{\max}}}{K_{n_p}^{q_{\max}}} > 0.5 \tag{29}$$

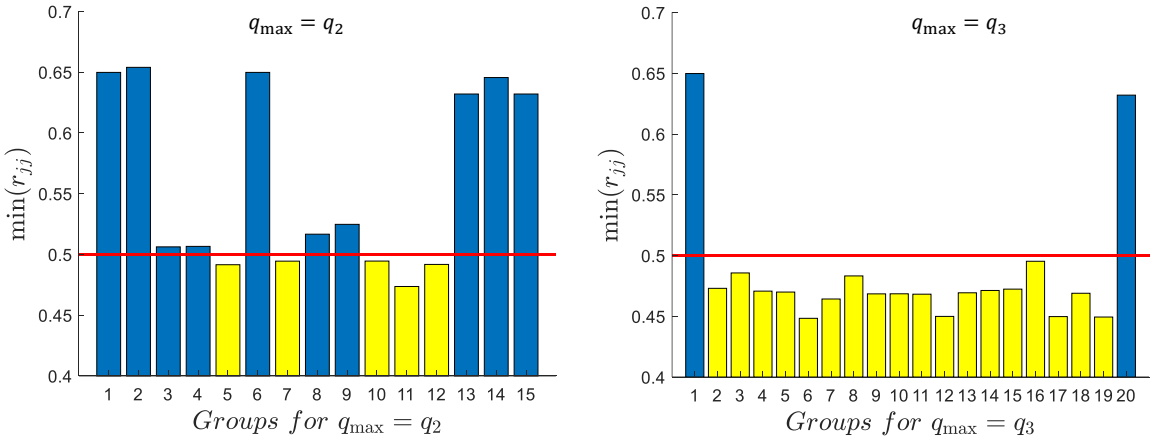

Fig. 5 Minimum redundancy numbers for q_2 and q_3.

Based on the average criterion mentioned above, for $q_{\max} = q_2$, we obtain $avg(\min r_{ll})_{g_i}^{q_2} = 0.56 > 0.5$, whereas for q_3, the result would be $avg(\min r_{ll})_{g_i}^{q_3} = 0.48 < 0.5$. Therefore, $q_{\max} = q_2$ could be considered; however, it can be observed that some groups for q_2 do not meet the criterion of $r_{jj} < 0.5$, which complicates the identification of these groups. For this reason, we recommend using the more stringent criterion to select $q_{\max}$ based on the minimum of the lowest r_{jj} values.

3 Results from computational simulation-based approach and real dataset: a trilateration geodetic network

For a first performance testing of the SeqCup-Free procedure, we use a simulated trilateration network measured in two epochs (Fig. 6), which is the same network presented in the previous sections (Fig. 1).

The network points are assumed to be stable at Epoch 1 (Table 1), so that the measurements connected to them are undisturbed (Table 2). Thus, the true quantities in Table (2) are stacked into a vector, such as in Eq.(1) $\boldsymbol{y_v}$.

To have simulated observations for Epoch 1 $\boldsymbol{y}^{(1)}$ – see Equation (1) –, the measurement errors are synthetically generated by assuming the presence of only random errors, whose is modeled by a multivariate normal distribution and added up to the true distances, as follows:

$$\boldsymbol{y}^{(1)} = \boldsymbol{y}_v^{(1)} + \boldsymbol{e_v}^{(1)}, \quad \text{with} \quad \boldsymbol{e_v}^{(1)} \sim N\left(\mathbf{0}, \boldsymbol{\Sigma}_{\boldsymbol{y}}^{(1)}\right) \tag{30}$$

The observations are assumed to be uncorrelated and with the same known standard deviation of $\sigma = 2\ mm$, which is a value compatible with real cases. Then the main diagonal elements of the variance matrix for the Epoch 1 are the variances

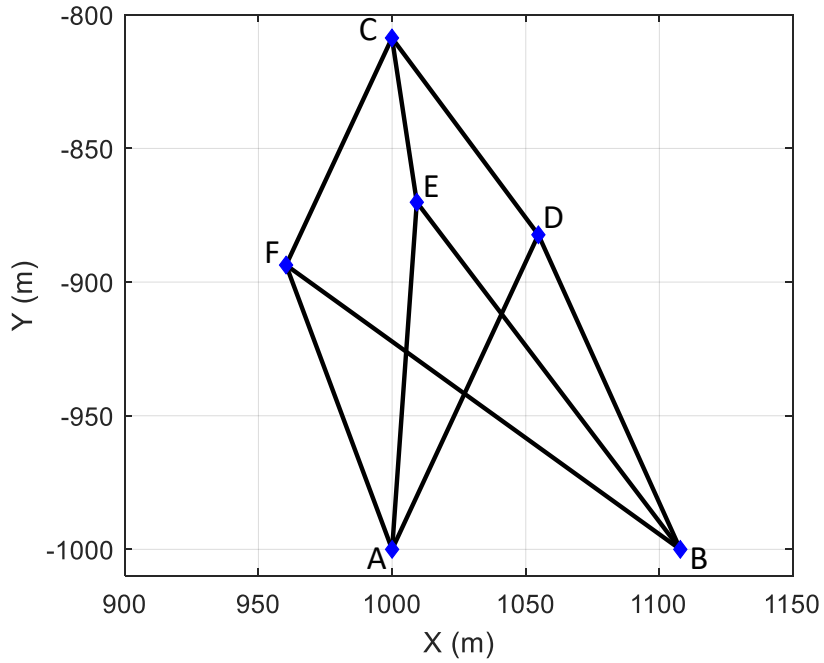

Fig. 6 Simulated Trilateration Network.

Table 1 Coordinates of the network points for Epoch 1

Point	X [m]	Y [m]
A	1000.000	-1000.000
B	1107.830	-1000.000
C	999.949	-808.661
D	1054.730	-882.298
E	1009.240	-870.129
F	960.330	-893.626

with values equal to $\sigma^2 = 4\ mm^2$, and its off-diagonal elements are zeros. Here, we use the Mersenne Twister algorithm to generate a sequence of random numbers and Box–Muller to transform it into a normal distribution Box and Muller (1958); Matsumoto and Nishimura (1998). For instance, Matlab's *mvnrnd* command can be applied to generate the random errors.

For Epoch 2, on the other hand, measurement distortions are simulated from the intentional displacement of the network points. The point displacements are simulated in terms of magnitude, denoted by ∇, and orientation, denoted by θ, so that they can be propagated to the distance. To illustrate this step, consider that the segment

Table 2 True distances of the segments for Epoch 1

Segment	True Distance [m]
$y_{v1}^{(1)} \equiv d_{v_{AD}}^{(1)}$	129.8025
$y_{v2}^{(1)} \equiv d_{v_{AE}}^{(1)}$	130.1994
$y_{v3}^{(1)} \equiv d_{v_{AF}}^{(1)}$	113.5303
$y_{v4}^{(1)} \equiv d_{v_{BD}}^{(1)}$	129.1275
$y_{v5}^{(1)} \equiv d_{v_{BE}}^{(1)}$	163.0530
$y_{v6}^{(1)} \equiv d_{v_{BF}}^{(1)}$	181.8570
$y_{v7}^{(1)} \equiv d_{v_{CD}}^{(1)}$	91.7765
$y_{v8}^{(1)} \equiv d_{v_{CE}}^{(1)}$	62.1665
$y_{v9}^{(1)} \equiv d_{v_{CF}}^{(1)}$	93.7482

formed by any two points i and j has suffered distortion when point i is displaced to its new position i' (Fig.7). In this case, the true disturbed distance in Epoch 2 is simulated as:

$$d_{v_{ij}}^{(2)} = \sqrt{\left(X_j - [X_i + \nabla_{X\,i}]\right)^2 + \left(Y_j - [Y_i + \nabla_{Y\,i}]\right)^2}, \quad i \neq j \tag{31}$$

with

$$\nabla_{X_i} = \nabla_i \sin\theta_i, \;\; \nabla_{Y_i} = \nabla_i \cos\theta_i \tag{32}$$

The true disturbed distances in Epoch 2 $\left(\boldsymbol{y}_v^{(2)}\right)$ can then be simulated as:

$$\boldsymbol{y_v}^{(2)} = \boldsymbol{y_v}^{(1)} + \boldsymbol{C}_{g_i}^{q_j} \boldsymbol{\nabla}_{g_i}^{q_j}, \quad i = 1, \ldots, K_{n_p}^{q_j} \tag{33}$$

Displacements can vary in terms of their magnitude ($\boldsymbol{\nabla}$) and orientation (θ), as well as the dimension q_j of the point group g_i. For the trilateration network in Fig. (6), for example, if we wanted to simulate the displacement of two points (i.e., q_2), then we would have a total of $K_6^{q_2} = 15$ groups of 2 points each. For each group, the magnitudes and directions of the displacements could also be simulated according to Eq. (31).

Next, the observations at the Epoch 2 are generated in the same way as it was done for Epoch 1, but now with the true disturbed distances $\left(\boldsymbol{y}_v^{(2)}\right)$, such as in Eq.(31), as follows:

$$\boldsymbol{y}^{(2)} = \boldsymbol{y}_v^{(2)} + \boldsymbol{e_v}^{(2)}, \quad \text{with} \quad \boldsymbol{e_v}^{(2)} \sim N\left(\boldsymbol{0}, \boldsymbol{\Sigma}_{\boldsymbol{y}}^{(2)}\right) \tag{34}$$

The variance matrix for the Epoch 2 is taken to be the same as in Epoch 1, i.e., $\boldsymbol{\Sigma}_{\boldsymbol{y}}^{(1)} = \boldsymbol{\Sigma}_{\boldsymbol{y}}^{(2)}$. Here, the value of σ is not relevant to this investigation.

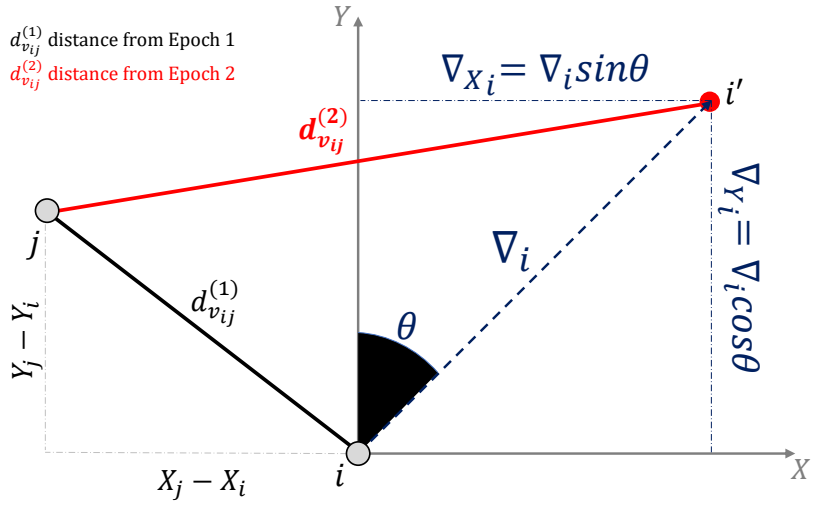

Fig. 7 Geometric aspect of simulating the displacement of a point and its effect on distance distortion.

Finally, the error vector $\boldsymbol{\Delta}\hat{\boldsymbol{e}}$ is computed according to Eq. (3). This process is repeated M times, meaning that M random events (known as Monte Carlo experiments) are generated for each desired scenario to evaluate the success and failure rates of the SeqCup-Free. For this numerical example, we set up $M = 200,000$ Monte Carlo experiments as suggested by Rofatto et al. (2020a).

The success and failure rates (also interpreted as probability levels) associated with SeqCup-Free (denoted by $\mathcal{P}[\cdot]$) were computed as the ratio between the occurrence of a particular event – correct detection, correct identification, wrong identification, overidentifications – and the number of possible cases (i.e., the total number of Monte Carlo experiments $M = 200,000$), as given by Rofatto et al. (2020b):

$$\mathcal{P}_{CI} = \frac{n_{CI}}{M} \tag{35}$$

$$\mathcal{P}_{CD} = \frac{n_{CD}}{M} \tag{36}$$

$$\mathcal{P}_{WI} = \frac{n_{WI}}{M} \tag{37}$$

$$\mathcal{P}_{OI+} = \frac{n_{OI+}}{M} \tag{38}$$

$$\mathcal{P}_{OI-} = \frac{n_{OI-}}{M} \tag{39}$$

where:

- n_{CD} – number of correct detections: this is the number of experiments in which the SeqCup-Free procedure correctly detects displacements. Inversely, we have the missed detection rate for the case where SeqCup-Free does not detect displacements, as follows:

$$\mathcal{P}_{MD} = \frac{n_{MD}}{M} = 1 - \mathcal{P}_{CD} \tag{40}$$

- n_{WI} – number of wrong identifications: this is the number of experiments in which SeqCup-Free flags the point group as being unstable, while the true unstable point group with the same dimension q_j remains unidentified.
- n_{OI+} – represents the number of events in which more points are identified as unstable than those actually displaced, and the truly displaced points are correctly included among the flagged points, along with additional points.
- n_{OI-} – represents the number of events in which more points are identified as unstable than those actually displaced, but none of the truly displaced points are included among the flagged points, meaning all identified points are incorrect.
- n_{CI} – number of correct identifications: this is the number of experiments in which SeqCup-Free correctly identifies the displaced points. In this case, we have the following relationship for the success rate of correct identification of the displaced point:

$$\exists(\mathcal{P}_{CI}) \in [0,1] \Leftrightarrow (\mathcal{P}_{CD}) > 0, \quad \text{thus} \tag{41}$$

$$\mathcal{P}_{CI} = \mathcal{P}_{CD} - (\mathcal{P}_{WI} + \mathcal{P}_{OI+} + \mathcal{P}_{OI-}) \tag{42}$$

3.1 Success and Failure Rates of SeqCup-Free: numerical example for q_1

As seen previously, when applying the criterion $\min\left(\min r_{ll}\right)_{g_i}^{q_{\max}} > 0.5$, we found $q_{\max} = q_1$. Therefore, for this criterion, it does not make sense to simulate more than one individual displacement simultaneously. Thus, this experiment is devoted to the case where only one displacement is considered. In that case, we had six groups individually simulated, namely $\{g_i \mid i = 1, 2, 3, \ldots, 6\}$, with each group consisting of only one point, i.e.: $g_1 = [A]$, $g_2 = [B]$, $g_3 = [C]$, $g_4 = [D]$, $g_5 = [E]$, $g_6 = [F]$. The magnitude of the displacement for each group $\{\nabla_{g_i}^{q_1} \mid i = 1, 2, 3, 4, 5, 6\}$ was defined within the interval of $[1, 10]\sigma$ with increments of 1σ, where σ is the standard deviation of the observation, taken as $\sigma = 2$ mm (as mentioned before). The displacements were simulated to act in different orientations. The displacement orientation θ was simulated for the range of $[0°, 355°]$ with $5°$ increments. As a result, we had ten magnitudes of displacement for each of the 72 orientations, totaling 720 simulated displacements for each point (Fig.8).

200,000 Monte Carlo experiments were generated for each of those 720 cases, totaling 144 million experiments for each point. It is important to remember that the simulated displacements of the points were converted to the observation space as in Eq. (31), which resulted in the corresponding disturbances in the measurements. Then, the Epoch 2 observations were generated from Eq. (33), considering those true disturbance distance observations. Finally, the probability levels associated with the SeqCup-Free method were computed as detailed before.

The critical values were obtained for cases having the following $\mathcal{P}_{FA}$: $\alpha = 0.001\,(c_\alpha = 16.7628)$; $\alpha = 0.01\,(c_\alpha = 12.3378)$; $\alpha = 0.05\,(c_\alpha = 9.1971)$ and $\alpha = 0.1\,(c_\alpha = 7.7882)$. These critical values were computed using two million Monte Carlo experiments such that a user-defined $\mathcal{P}_{FA}$ α for SeqCup-Free was warranted (see Appendix B).

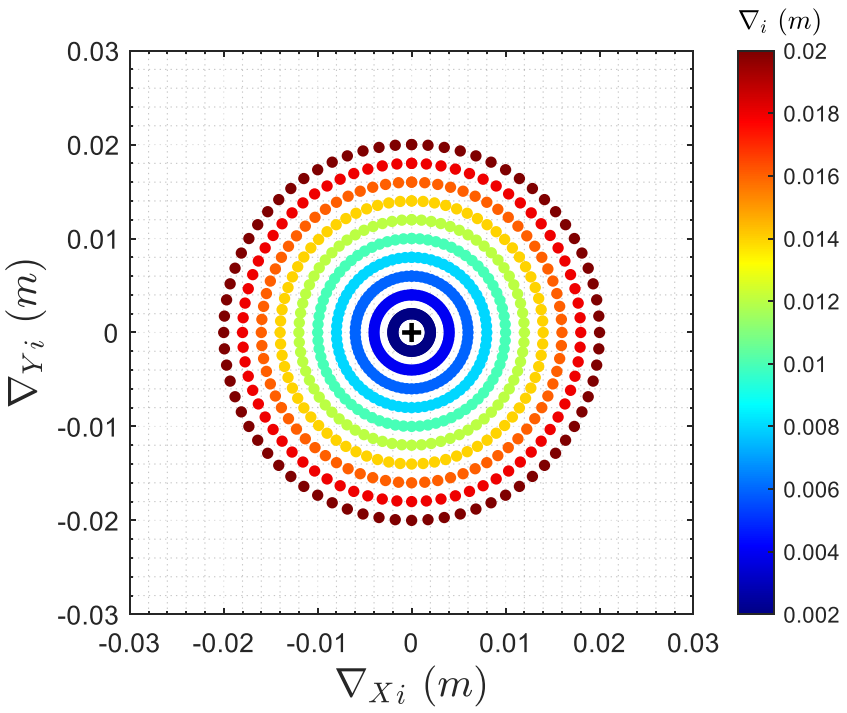

Fig. 8 Simulated displacements for each point at time (case q_1)

.

Figure 9 shows the result of the correct identification. The black circles represent the radial range of displacement magnitudes of 4 mm, 1 cm, and 2 cm. It is important to note that the uncertainty of the differences between the two-epoch geodetic observations is $\sigma_{\Delta\hat{e}} \approx 2.83$ mm. Therefore, these magnitudes of 4 mm, 1 cm, and 2 cm correspond to approximately $1.4\sigma_{\Delta\hat{e}}$, $3.5\sigma_{\Delta\hat{e}}$, and $7.1\sigma_{\Delta\hat{e}}$, respectively.

Clearly, it is observed that the probability of correct identification depends on the geometry of the connections. Note that the highest success rates occur along the lines of sight. On the other hand, it is more difficult to identify in directions perpendicular to the lines of sight, mainly for magnitudes close to the uncertainty of the measurement method ($\nabla \leq 4\,\text{mm}$). The increase in the significance level, and consequently a larger null hypothesis rejection region (smaller critical values), favors the identification of low-magnitude displacements. On the other hand, higher significance levels slightly reduce the probability of correctly identifying displacements of larger magnitudes.

Figure (10) shows the result of the correct detection. Detection follows the same behaviour as identification in terms of the influence of the geometry of the point connections. There are no significant differences in terms of detection and identification for the case in which a low significance level is adopted ($\alpha = 0.001$). The lower the critical value (higher significance level) the higher the detection rate.

In a trilateration network, the success rate of correct identification, as well as detection, is directly related to the spatial distribution of points and their connections

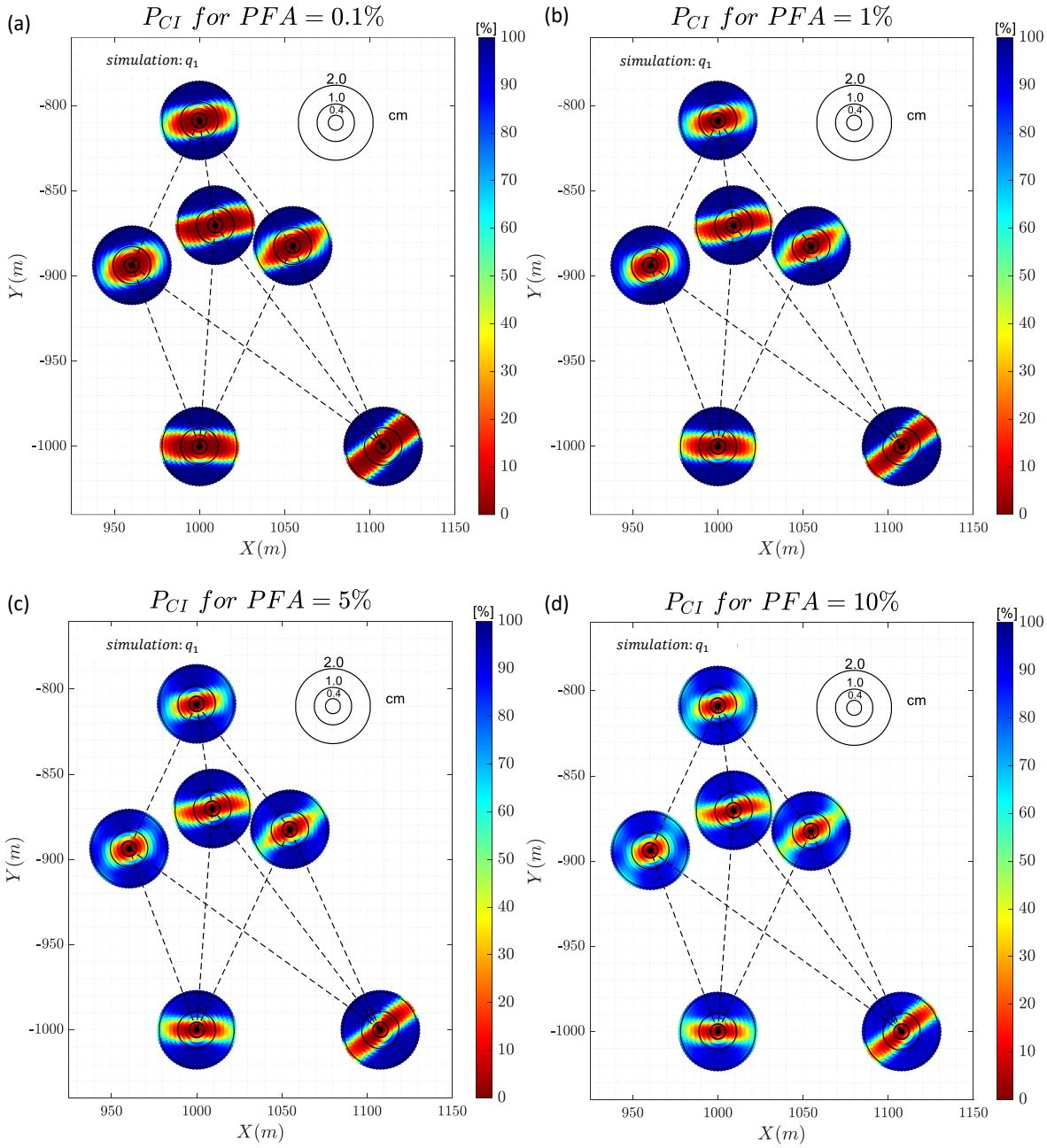

Fig. 9 Probability of correct identification ($\mathcal{P}_{CI}$): (a) $\mathcal{P}_{CI}$ for $\alpha = 0.1\%$; (b) $\mathcal{P}_{CI}$ for $\alpha = 1\%$; (c) $\mathcal{P}_{CI}$ for $\alpha = 5\%$; and (d) $\mathcal{P}_{CI}$ for $\alpha = 10\%$.

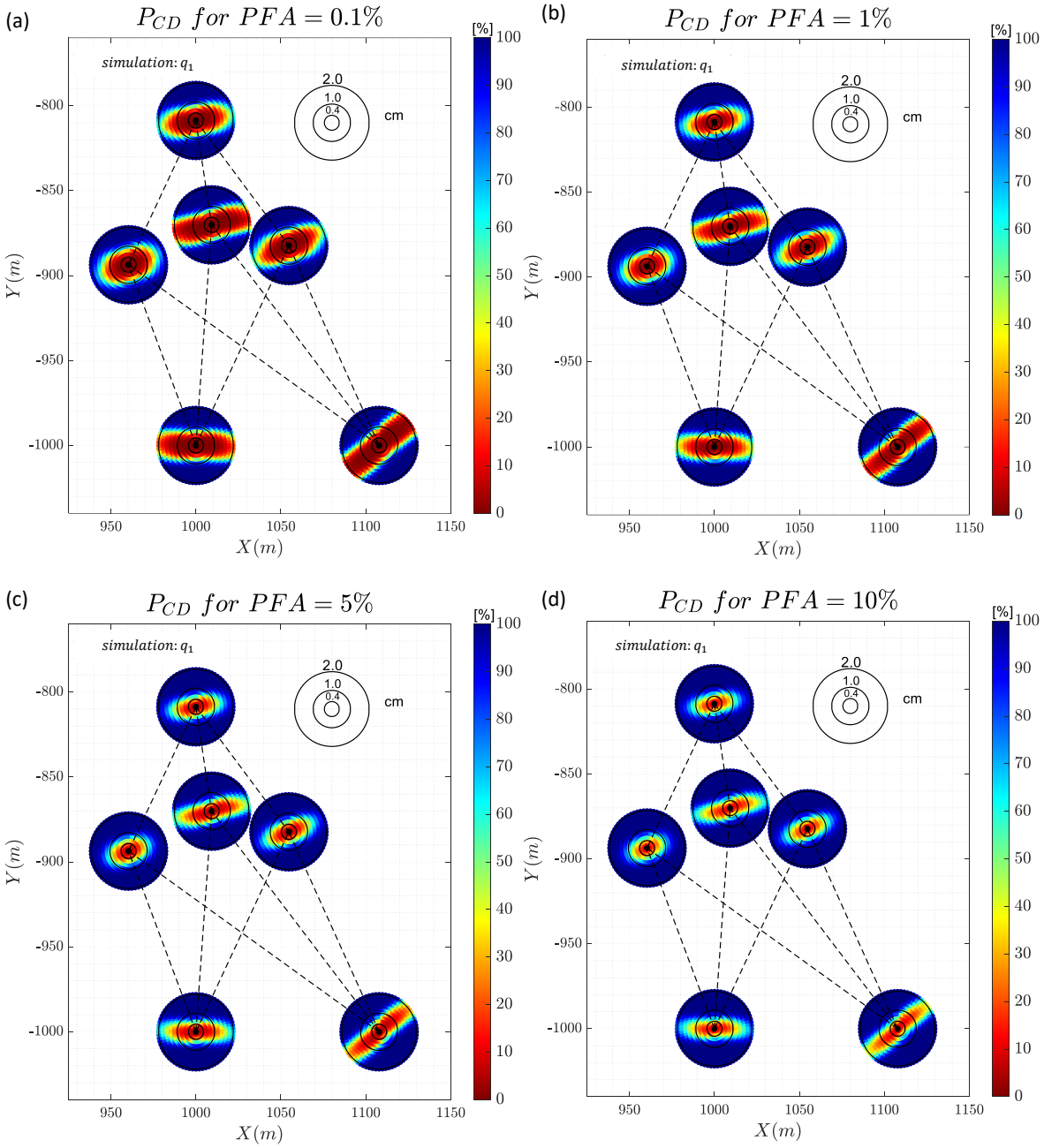

Fig. 10 Probability of correct detection ($\mathcal{P}_{CD}$): (a) $\mathcal{P}_{CD}$ for $\alpha = 0.1\%$; (b) $\mathcal{P}_{CD}$ for $\alpha = 1\%$; (c) $\mathcal{P}_{CD}$ for $\alpha = 5\%$; and (d) $\mathcal{P}_{CD}$ for $\alpha = 10\%$.

(Fig. 11). For example, the line-of-sight distances from points D, E, and F to point A can be considered as the radii of circles where D, E, and F are the centers, and A lies on the circumference. Figure (11)(a) highlights the locations where these circles intersect at point A. The dark red region represents the area where all three circles overlap, meaning that if point A moves within this region, detection and identification become impossible. The red areas indicate intersections of two circles, making detection more difficult for small displacements, as shown in the figure. The green region is an example where no three-circle intersection occurs, facilitating detection and identification. This behavior can also be observed for the other points in the network, where similar geometric constraints influence the detection and identification of displacements (see Figures 9 and 10). Therefore, the success rates are influenced not only by the proposed method but also by the spatial configuration of the network.

Figure (12) shows the results for wrong identification (also referred to as Type III decision error). This type of error becomes more significant as the level α increases. In the worst case, we have $\mathcal{P}_{WI} \cong 0.4$ (40%) for the scenario where point E is displaced and $\alpha = 0.01$. In general, wrong identification occurs at large magnitudes in the region outside the lines of sight.

The overidentification class $\mathcal{P}_{OI+}$ is presented in Figure (13). In general, this probability level becomes more evident with increasing α. The overidentification $\mathcal{P}_{OI-}$ was much rarer, with its highest value of $\mathcal{P}_{OI-} \cong 0.022$ (2.2%) for $\alpha = 0.1$, and thus is not shown here. On the other hand, positive overidentification $\mathcal{P}_{OI+}$ seems to occur more frequently than $\mathcal{P}_{OI-}$, especially close to the lines of sight and for large magnitudes.

In general, increasing α improved identification in the case of small (4mm) and medium (1cm) magnitudes of displacement. The impact of the α choice on the correct identification rate is not as critical for large magnitudes. Detection always improves as the critical region expands (i.e., as the critical value decreases), at the cost of having to increase false positive rates α. In the next section, we present the testing performance of the SeqCup-Free for the case of having 2 points displaced simultaneously.

3.2 Success and Failure Rates of SeqCup-Free: numerical example for q_2

As shown previously, by applying the criterion $\text{avg}\,(\min r_{ll})_{g_i}^{q_{\max}} > 0.5$, we found $q_{\max} = q_2$. Thus, with this less restrictive criterion compared to the previous one, we are able to simulate two individual displacements simultaneously. For this, we simulated all possible cases for q_2 one at a time, which resulted in 15 groups of 2 points individually simulated for the network in Fig.(6), denoted by $\{g_i \mid i = 1, 2, 3, \ldots, 15\}$. It is important to emphasize that the group of points was not randomized. Instead, the simulation for each group was performed individually in a more comprehensive manner, with each group undergoing 200,000 Monte Carlo experiments and the same false alarm level of $\alpha = 0.1$ ($c_\alpha = 7.7882$). The displacements were generated with a fixed magnitude of $5\sigma = 1\,\text{cm}$ for five distinct orientation patterns for each two-point group, denoted by $[\theta_{p_1}, \theta_{p_2}]$ as $[0°, 0°]$, $[0°, 180°]$, $[135°, 135°]$, $[135°, 315°]$, and $[315°, 315°]$. The success and failure rates for these patterns are presented in Tables 3, 4, 5, and 6, respectively. $\mathcal{P}_{UI+}$ and $\mathcal{P}_{UI-}$ both correspond to the identification rate

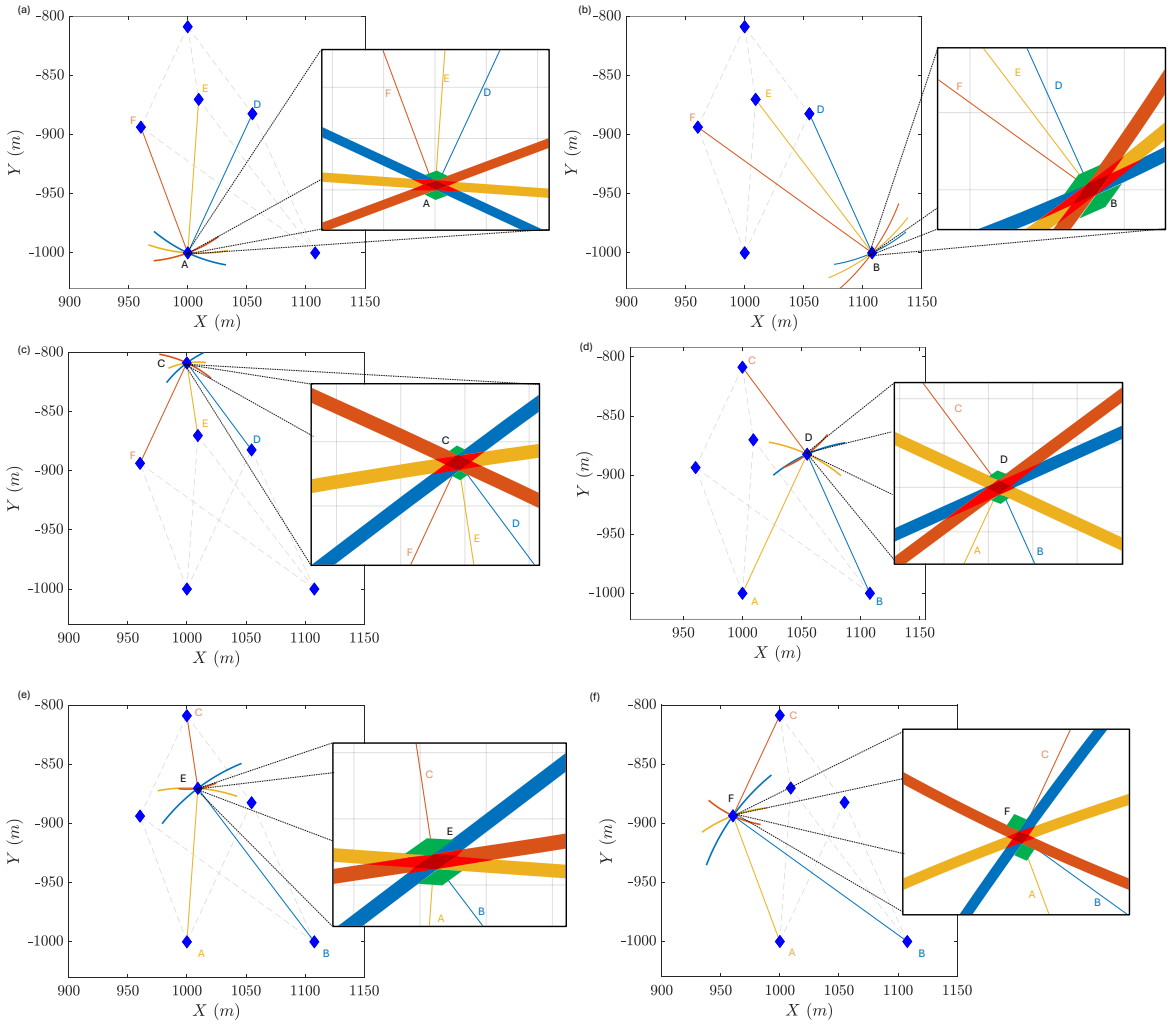

Fig. 11 Regions of intersection of trilateration circles for each network point (A to F). The dark red region corresponds to the area where all three circles intersect, which makes the displacement detection unfeasible. The red regions indicate intersections of two circles, where detection becomes more difficult for small displacements. The green regions represent areas without triple-circle intersections, which improves displacement detection and identification.

where fewer points are identified than the actual number of displaced points. The difference between them is that in $\mathcal{P}_{UI+}$, the identified set includes some of the truly displaced points, while in $\mathcal{P}_{UI-}$, none of the identified points correspond to the true displaced ones.

In terms of detection and identification success rates, the SeqCup-Free method depends on the interaction between the displacement pattern and the geometry of the geodetic network. One geometry may be more suitable for a given displacement

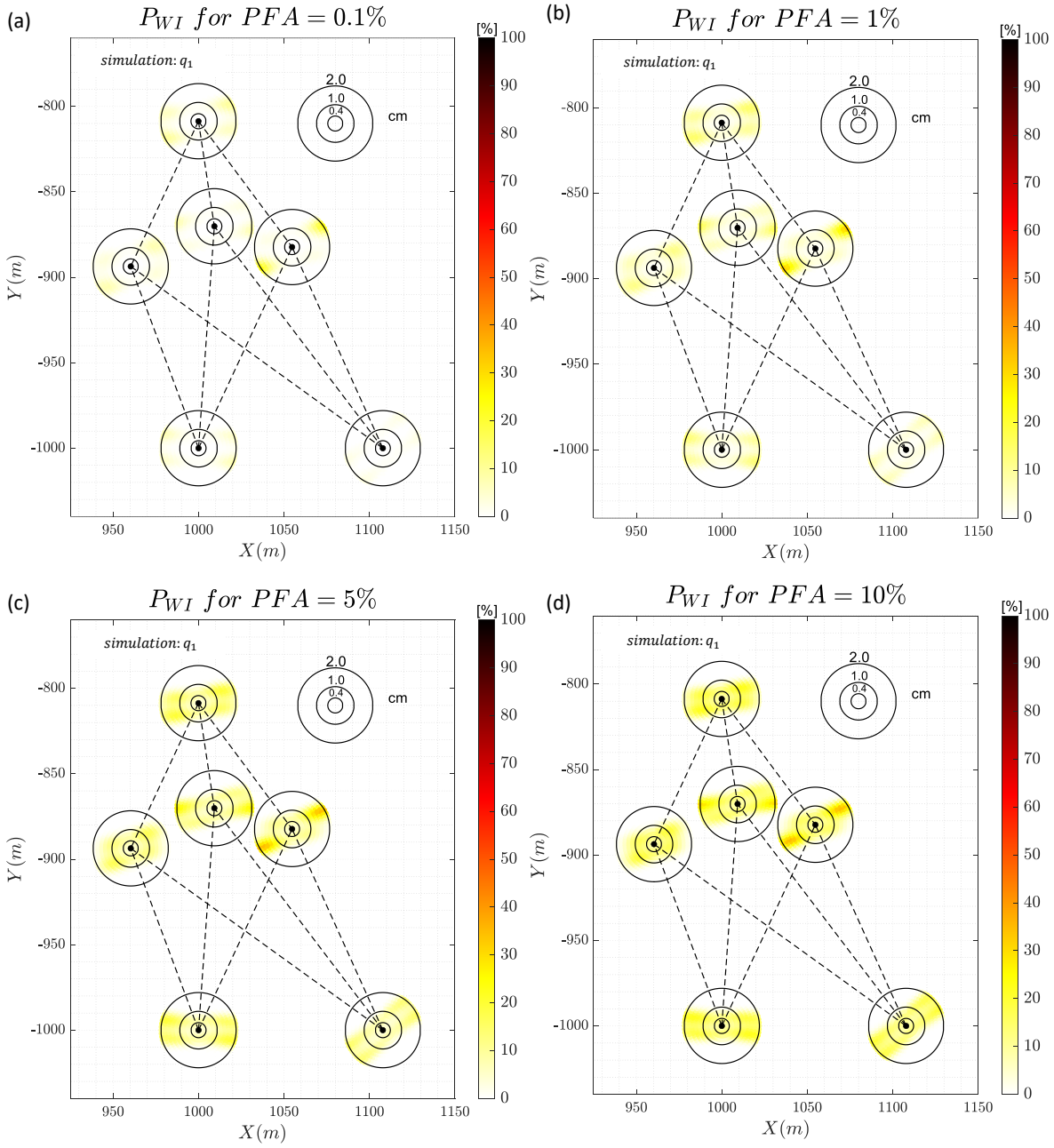

Fig. 12 Probability of wrong identification ($\mathcal{P}_{WI}$): (a) $\mathcal{P}_{WI}$ for $\alpha = 0.1\%$; (b) $\mathcal{P}_{WI}$ for $\alpha = 1\%$; (c) $\mathcal{P}_{WI}$ for $\alpha = 5\%$; and (d) $\mathcal{P}_{WI}$ for $\alpha = 10\%$.

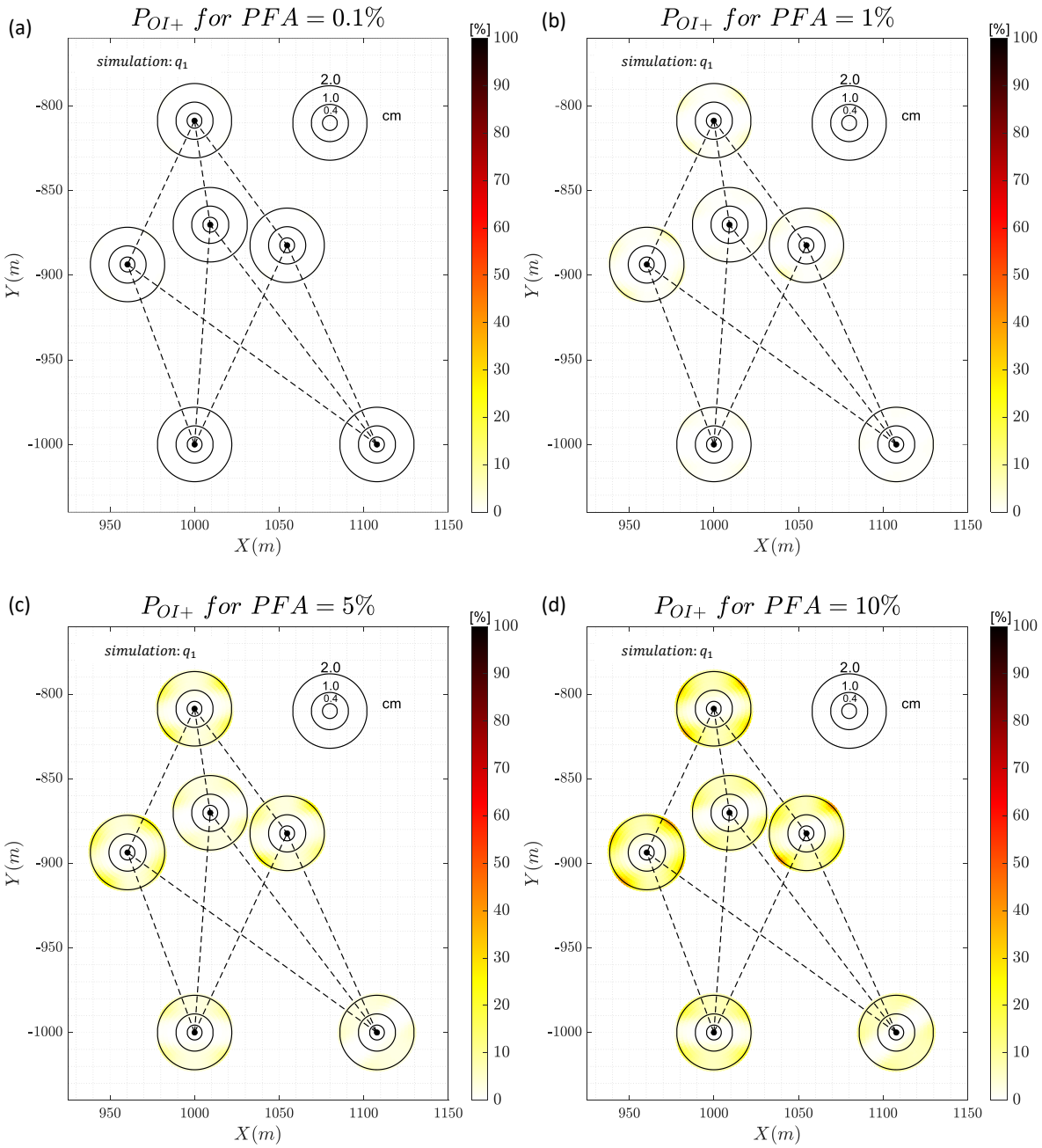

Fig. 13 Probability of wrong identification ($\mathcal{P}_{OI+}$): (a) $\mathcal{P}_{OI+}$ for $\alpha = 0.1\%$; (b) $\mathcal{P}_{OI+}$ for $\alpha = 1\%$; (c) $\mathcal{P}_{OI+}$ for $\alpha = 5\%$; and (d) $\mathcal{P}_{OI+}$ for $\alpha = 10\%$.

Table 3 Success and Failure Rates for $\theta_{p_1} = 0°$ and $\theta_{p_2} = 0°$

Group	p_1	p_2	$\mathcal{P}_{CI}$	$\mathcal{P}_{CD}$	$\mathcal{P}_{MD}$	$\mathcal{P}_{WI}$	$\mathcal{P}_{UI+}$	$\mathcal{P}_{UI-}$
1	1	2	81.35	99.98	0.02	4.38	9.16	5.09
2	1	3	89.03	100.00	0.00	3.13	1.72	6.12
3	1	4	5.17	98.76	1.24	39.24	51.09	3.26
4	1	5	4.28	98.73	1.27	40.80	50.29	3.36
5	1	6	1.74	97.32	2.68	33.84	55.70	6.04
6	2	3	79.75	99.96	0.04	4.81	9.22	6.18
7	2	4	1.22	93.49	6.51	23.09	60.56	8.62
8	2	5	2.94	98.58	1.42	35.47	56.43	3.74
9	2	6	5.71	98.22	1.78	35.31	53.63	3.57
10	3	4	4.53	99.24	0.76	44.53	46.91	3.27
11	3	5	1.71	97.45	2.55	37.92	51.94	5.88
12	3	6	1.83	97.49	2.51	36.33	52.65	6.68
13	4	5	88.40	100.00	0.00	2.93	3.16	5.51
14	4	6	81.93	99.96	0.04	4.83	5.68	7.52
15	5	6	81.20	100.00	0.00	5.79	4.97	8.04

pattern that one wishes to monitor. For example, the patterns $[\theta_{p_1} = 0°; \theta_{p_2} = 0°]$ and $[\theta_{p_1} = 315°; \theta_{p_2} = 315°]$ in Tables 3 and 6, respectively, exhibited a higher number of point groups with low identification rates, whereas the patterns $[\theta_{p_1} = 0°; \theta_{p_2} = 180°]$ and $[\theta_{p_1} = 135°; \theta_{p_2} = 315°]$ in Tables 4 and 5, respectively, had more point groups correctly identified. This is because the displacements occur close to the lines of sight (regions where identification is easier), as demonstrated in the previous section for the case of q_1. Additionally, displacement patterns with pairs of points moving in different directions seem to be easier to identify, and no statistical overlap was observed. It is also noted that the relationship between the network geometry and the displacement pattern can either increase or decrease the rates of wrong identification and underidentification.

It is important to highlight that detection is always greater than or at least equal to identification. In this sense, we also observe that the detection rate was very high ($\approx 98\%$ on average), which allows us to infer that failures to detect the displacement patterns simulated here are very rare.

3.3 Success and Failure Rates of SeqCup-Free for Simulated Displacement Based on Real Dataset

In this experiment, the geodetic network described in Fig.(6) was materialized in the field. The distances were measured using a total station with a linear uncertainty of 2mm + 2ppm (according to the manufacturer's specifications). Tribrachs were used for both the total station and the reflector prisms. These data are available

Table 4 Success and Failure Rates for $\theta_{p_1} = 0°$ and $\theta_{p_2} = 180°$

Group	p_1	p_2	$\mathcal{P}_{CI}$	$\mathcal{P}_{CD}$	$\mathcal{P}_{MD}$	$\mathcal{P}_{WI}$	$\mathcal{P}_{UI+}$	$\mathcal{P}_{UI-}$
1	1	2	80.79	99.96	0.04	4.41	9.37	5.39
2	1	3	88.93	100.00	0.00	2.89	2.02	6.16
3	1	4	89.79	100.00	0.00	4.21	6.00	0.00
4	1	5	94.46	100.00	0.00	2.43	3.11	0.00
5	1	6	85.78	100.00	0.00	4.56	9.66	0.00
6	2	3	78.83	99.96	0.04	5.62	9.37	6.14
7	2	4	79.86	100.00	0.00	4.22	15.92	0.00
8	2	5	71.24	100.00	0.00	10.11	18.65	0.00
9	2	6	57.96	99.99	0.01	16.32	25.68	0.03
10	3	4	85.92	100.00	0.00	6.41	7.67	0.00
11	3	5	94.59	100.00	0.00	2.16	3.25	0.00
12	3	6	86.10	100.00	0.00	5.38	8.52	0.00
13	4	5	88.54	99.99	0.01	2.99	3.24	5.22
14	4	6	82.82	99.96	0.04	4.09	5.64	7.41
15	5	6	80.74	99.96	0.04	5.72	5.23	8.27

Table 5 Success and Failure Rates for $\theta_{p_1} = 135°$ and $\theta_{p_2} = 315°$

Group	p_1	p_2	$\mathcal{P}_{CI}$	$\mathcal{P}_{CD}$	$\mathcal{P}_{MD}$	$\mathcal{P}_{WI}$	$\mathcal{P}_{UI+}$	$\mathcal{P}_{UI-}$
1	1	2	66.35	99.86	0.14	9.18	18.57	5.75
2	1	3	58.86	99.19	0.81	6.39	22.36	11.58
3	1	4	21.31	99.67	0.33	29.96	47.47	0.93
4	1	5	45.72	99.96	0.04	16.97	37.24	0.03
5	1	6	68.83	99.99	0.01	5.01	26.15	0.00
6	2	3	76.81	99.96	0.04	7.01	7.94	8.20
7	2	4	80.10	100.00	0.00	7.88	12.02	0.00
8	2	5	88.38	100.00	0.00	3.58	8.04	0.00
9	2	6	78.68	100.00	0.00	7.07	14.25	0.00
10	3	4	85.32	100.00	0.00	3.81	10.87	0.00
11	3	5	71.05	100.00	0.00	11.28	17.67	0.00
12	3	6	26.60	99.83	0.17	33.32	39.39	0.52
13	4	5	64.11	99.92	0.08	12.84	10.02	12.95
14	4	6	65.63	99.69	0.31	8.89	11.81	13.36
15	5	6	67.87	99.81	0.19	10.30	10.68	10.96

Table 6 Success and Failure Rates for $\theta_{p_1} = 315°$ and $\theta_{p_2} = 315°$

Group	p_1	p_2	$\mathcal{P}_{CI}$	$\mathcal{P}_{CD}$	$\mathcal{P}_{MD}$	$\mathcal{P}_{WI}$	$\mathcal{P}_{UI+}$	$\mathcal{P}_{UI-}$
1	1	2	66.55	99.93	0.07	8.52	18.70	6.16
2	1	3	59.51	99.14	0.86	6.50	21.93	11.20
3	1	4	3.05	98.28	1.72	36.61	54.33	4.29
4	1	5	1.06	94.59	5.41	31.54	53.46	8.53
5	1	6	0.17	74.21	25.79	12.24	39.44	22.36
6	2	3	76.52	99.98	0.02	7.39	8.03	8.04
7	2	4	1.29	96.72	3.28	37.10	51.80	6.53
8	2	5	3.14	97.00	3.00	31.94	57.19	4.73
9	2	6	1.51	96.32	3.68	33.53	54.37	6.91
10	3	4	0.13	82.07	17.93	19.48	39.28	23.18
11	3	5	0.52	92.85	7.15	31.67	45.55	15.11
12	3	6	4.24	98.86	1.14	41.88	49.18	3.56
13	4	5	64.56	99.82	0.18	13.29	9.55	12.42
14	4	6	65.49	99.73	0.27	9.52	11.70	13.02
15	5	6	67.37	99.86	0.14	9.82	11.22	11.45

from the authors upon request, either to reproduce the experiments or to test other procedures. Epoch 1 was recorded as the baseline with no displacements, while in Epoch 2, various displacement patterns were tested. The displacements at the points were applied radially and intentionally. Points A, B, and C were kept fixed, meaning they were not subjected to displacement, whereas points D, E, and F were considered the points to be monitored. Displacements were performed in the field by moving the reflector 1 cm from its initial position (Epoch 1) to the new positions (Epoch 2), as shown in Figure (14). Four cases involved shifting only one point at a time, as displayed in Fig.(14 a,b,c,d); three scenarios involved 2 or 3 simultaneous displacements, with the patterns shown in Fig.(13 e,f,g) and Fig.(14 h,i,j), respectively, totaling 23 experiments (12 for q_1, 8 for q_2, and 3 for q_3). As previously noted, the network would have a maximum capacity of $q_{\max} = q_2$ according to the more flexible criterion (Equation 29), but here we also extended the evaluation to $q_{\max} = q_3$.

Based on the simulated results, we adopted a significance level of $\alpha = 0.1$, which resulted in a critical value of $c_\alpha = 7.7882$. The results are very promising, as can be seen in Table (7). We had a success rate in the identification of $\approx 82.61\%$, and the correct detection rate was 100% for all scenarios.

Finally, SeqCup-Free was applied in a scenario where no displacements occurred to verify the efficiency of $\mathcal{P}_{FA}$ control for $\alpha = 0.1$. New measurements were performed and recorded as Epoch 2, but without applying any intentional displacement to the points. As a result, no displacements were detected in the field experiments, indicating that SeqCup-Free could guarantee the user-defined $\mathcal{P}_{FA}$ under real conditions of use.

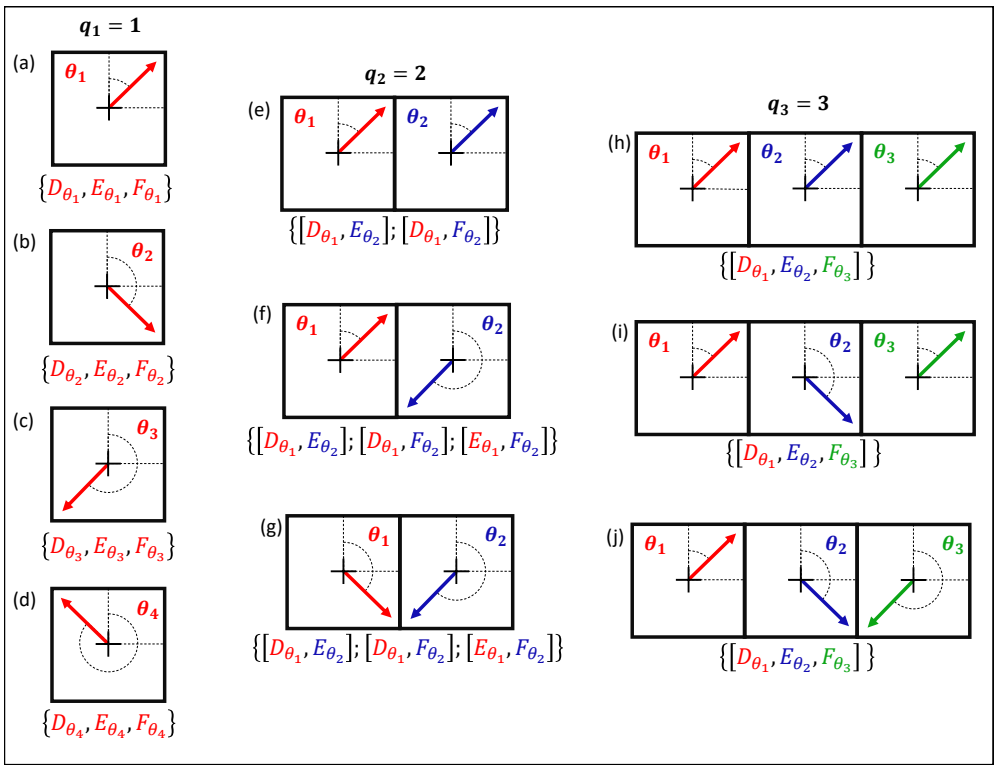

Fig. 14 Displacement patterns applied in the field: (a) displacement of each individual point in the θ_1 direction, denoted by D_{θ_1}, E_{θ_1}, F_{θ_1}; (b) displacement of each individual point in the θ_2 direction, denoted by D_{θ_2}, E_{θ_2}, F_{θ_2}; (c) displacement of each individual point in the θ_3 direction, denoted by D_{θ_3}, E_{θ_3}, F_{θ_3}; (d) displacement of each individual point in the θ_4 direction, denoted by D_{θ_4}, E_{θ_4}, F_{θ_4}; (e, f, g) simultaneous displacement of two-point groups, with the first point shifted in the θ_1 direction and the second in the θ_2 direction; (h, i, j) simultaneous displacement of three-point groups, with the first point shifted in the θ_1 direction, the second in the θ_2 direction, and the third in the θ_3 direction.

4 External Validation from Classical and Recent Methods

4.1 Numerical Example 1: GCT, V, AICc and CIDIA

Here, we compare the suggested SeqCup-Free method with the classical iterative GCT (Global Congruence Test), the combinatorial method V — Velsinki method (Velsink 2015), Akaike's Information Criterion with correction (AICc) suggested by Lehmann and Lösler (2017), and the more recent Combinatorial Iterative Detection, Identification, and Adaptation (CIDIA) by Nowel (2020). The GCT belongs to the class of iterative methods, V and AICc are combinatorial methods, while CIDIA encompasses both combinatorial and iterative approaches. Nowel (2020) provided a detailed description of each method, and thus they will not be presented again here. For further

Table 7 Frequency of occurrence for each SeqCup-Free decision class for the real dataset case.

Displacement patterns	n_{CD}	n_{CI}	n_{WI}	n_{UI+}
(a)	3	3	0	0
(b)	3	3	0	0
(c)	3	3	0	0
(d)	3	3	0	0
(e)	2	1	0	1
(f)	3	1	0	2
(g)	3	3	0	0
(h)	1	0	1	0
(i)	1	1	0	0
(j)	1	1	0	0
Total	23	19	1	3
Rate (%)	100	82.61	4.35	13.04

reference, the reader can consult Section 2.1 for GCT, Section 2.2 for the V method and AICc, and Section 3 for CIDIA in the work of Nowel (2020).

For comparative purposes, we used the same network from Lehmann and Lösler (2017), adapted by Nowel (2020), to meet redundancy criteria (Fig. 15). The experiments were conducted with the same configuration to allow for a direct comparison of results. The concept of Mean Success Rate (MSR), as proposed by Hekimoglu and Koch (1999), was also applied here, with the same simulation setup as in Nowel's experiments, to measure the efficacy of correct model specification. Specifically, errors were randomized from a Normal distribution across two epochs with a known standard deviation $\sigma = 1\,\text{mm}$, while point displacements were randomized from the uniform interval $\nabla_i \in [2 - 25]\,\text{mm}$, all with the same sign. The vectors of 2×29 height difference errors were simulated independently 1000 times using MATLAB software, as per Nowel (2020). Additionally, 50 trials (repetitions) of these 1000 Monte Carlo experiments were conducted to account for the uncertainty of the simulation process ($\pm\sigma_{MC}\%$), such as in Rofatto et al. (2020a). This process enables comparison with the results found in the cited literature.

For each simulation, four scenarios were considered in terms of the number of displaced points, namely: one (q_1), two (q_2), four (q_4), and six (q_6) points randomly selected to be displaced. According to the criterion $\min\left(\min r_{ll}\right)_{g_i}^{q_{\max}} > 0.5$, we found that for this network, $q_{\max} = 10$, indicating that this network has excellent redundancy for monitoring purposes. The $\mathcal{P}_{FA}$ for SeqCup-Free was set to $\alpha = 0.001$, $\alpha = 0.01$, $\alpha = 0.05$, and $\alpha = 0.1$, with their corresponding critical values $c_\alpha = 15.4055$, $c_\alpha = 11.1467$, $c_\alpha = 8.1480$, and $c_\alpha = 6.8213$, obtained from the Monte Carlo Approach in Appendix (B) for 2,000,000 Monte Carlo experiments. The results are displayed in Table (8).

Table 8 Efficacy (MSR with $\pm\sigma_{MC}\%$) of the SeqCup-Free for different $\mathcal{P}_{FA}$ and number of displaced points

$\mathcal{P}_{FA}$	c_α	q_1	q_2	q_4	q_6
0.001	15.4055	96.6 ± 0.6	93.1 ± 0.8	83.5 ± 1.2	61.3 ± 1.6
0.01	11.1467	97.1 ± 0.5	94.8 ± 0.7	87.9 ± 1.0	67.3 ± 1.3
0.05	8.1480	94.1 ± 0.8	93.3 ± 0.7	88.6 ± 1.0	70.1 ± 1.4
0.1	6.8213	89.7 ± 1.0	89.8 ± 1.0	86.5 ± 1.1	70.5 ± 1.1

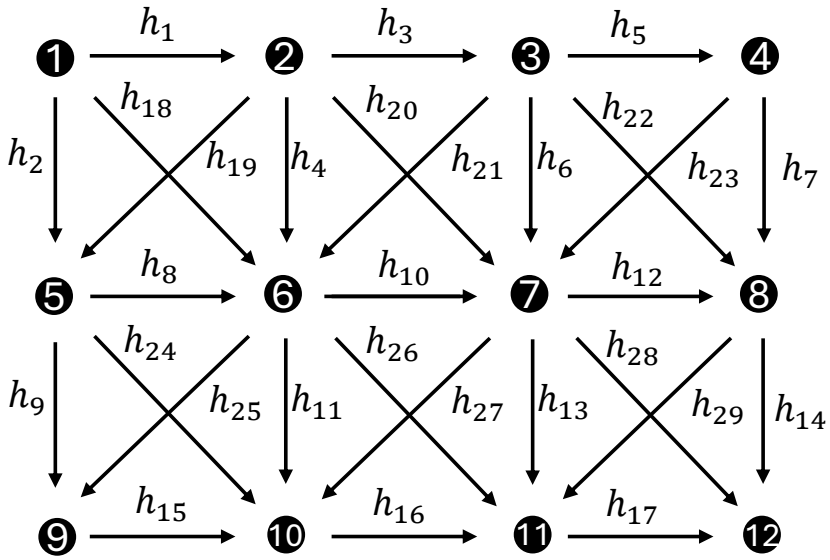

Fig. 15 Configuration of the leveling control network based on Lehmann and Lösler (2017) and adapted by Nowel (2020)

As can be seen, lower values of α are more suitable when fewer displacements are expected (q_1 and q_2), while higher values of α are preferable for scenarios with more displacements (q_4 and q_6). However, the value of $\alpha = 0.01$ appears to be a balanced choice for different scenarios, offering high efficacy for both small and large numbers of displacements for this experiment. The use of Monte Carlo simulations is an excellent strategy for determining the optimal $\mathcal{P}_{FA}$ before conducting field observations. This process allows for a careful evaluation of the method's efficacy for different configurations, which enables the selection of an α that maximizes reliability.

The results from Nowel (2020) were replicated in Table 9, and the result of the SeqCup-Free method with the same $\alpha = 0.1$, as adopted by Nowel, was added for comparison purposes (denoted as SeqCup only), which ensures compatibility in the comparisons. In this experiment, we also evaluated a modified version of SeqCup-Free (denoted by SeqCupMod), which dispenses with the step of assessing whether the

null hypothesis is a subset of the alternative hypothesis. This approach follows the framework of non-nested hypothesis testing, unlike the original method, which uses nested hypothesis testing.

In the case of non-nested models, we applied the concept of the Akaike Information Criterion (AIC) with a penalty for the number of parameters, as follows (Lehmann and Lösler 2017):

$$AICc = AIC + \frac{2u(u+1)}{n-u-1} \tag{43}$$

with

$$AIC = 2u - 2\log L(\hat{\theta}; \boldsymbol{\Delta_y}) \tag{44}$$

where L denotes the likelihood function of the model, which is maximized by the maximum likelihood (ML) estimate $\hat{\theta}$ of the u-vector of parameters θ with respect to the observations $\boldsymbol{\Delta_y}$.

In our case, the GLRT in Eq. (17) is replaced by the AIC for the null and alternative hypotheses, respectively, as follows:

$$AICc_{(\mathcal{H}_0)} = 2q_j + \frac{2q_j(q_j+1)}{n-q_j-1} + \underbrace{\left(\boldsymbol{\Delta}\hat{\boldsymbol{e}}_{g_i}^{q_j}\right)^{\top} \boldsymbol{W} \left(\boldsymbol{\Delta}\hat{\boldsymbol{e}}_{g_i}^{q_j}\right)}_{\mathcal{H}_0} \tag{45}$$

$$AICc_{(\mathcal{H}_A)} = 2q_{j+1} + \frac{2q_{j+1}(q_{j+1}+1)}{n-q_{j+1}-1} + \underbrace{\left(\boldsymbol{\Delta}\hat{\boldsymbol{e}}_{g_k}^{q_{j+1}}\right)^{\top} \boldsymbol{W} \left(\boldsymbol{\Delta}\hat{\boldsymbol{e}}_{g_k}^{q_{j+1}}\right)}_{\mathcal{H}_A} \tag{46}$$

The criterion is as follows: Among the null and alternative models under consideration, the one with the lowest AICc should be selected. This ensures a high likelihood while limiting the number of parameters, which prevents overfitting.

The comparison of SeqCup and SeqCupMod with other methods is described as follows:

GCT: Taking into account the simulation standard deviation for q_1, q_2, and q_4, SeqCup is largely consistent with GCT.

- For q_1, SeqCup (89.7% ±1.0) is considered identical to GCT (89.8%), since the difference falls within the simulation uncertainty, indicating full compatibility between the two methods. SeqCupMod achieves a slightly higher score (89.9% ±1.0), which remains consistent with GCT.

- For q_2, SeqCup (89.8% ±1.0) remains highly compatible with GCT (87.8%), with the standard deviation showing that both methods perform similarly. SeqCupMod (89.6% ±1.0) also maintains similar compatibility. - For q_4, SeqCup (86.5% ±1.1) aligns closely with GCT (86.2%), and SeqCupMod performs even better (88.8% ±1.1), showing improved results compared to both SeqCup and GCT.

Hence, SeqCup and SeqCupMod are compatible with GCT for q_1, q_2, and q_4. However, for q_6, SeqCup shows a lower performance compared to GCT (70.5% ±1.1 versus 74.1%), while SeqCupMod improves significantly, reaching 87.4% ±1.1, surpassing both GCT and SeqCup.

CIDIA: SeqCup is relatively close to CIDIA for q_1, q_2, and q_4. However, for q_6, CIDIA outperforms SeqCup significantly (88.5% versus 70.5%). SeqCupMod, on the other hand, closes the gap, performing closely to CIDIA with 87.4%.

Table 9 Efficacy (MSR) of correct model specification for different methods of model specification based on Nowel (2020) [%].

Number of displaced points	GCT	V	AICc	CIDIA	SeqCup$_{(\alpha=0.1)}$	SeqCupMod$_{(\alpha=0.1)}$
1/12 (q_1)	89.8	92.9	54.2	90.6	89.7 ±1.0	89.9 ±1.0
2/12 (q_2)	87.8	69.4	59.2	89.4	89.8 ±1.0	89.6 ±1.0
4/12 (q_4)	86.2	23.0	69.8	88.4	86.5 ±1.1	88.8 ±1.1
6/12 (q_6)	74.1	9.5	80.5	88.5	70.5 ±1.1	87.4 ±1.1

V (Velsinki method): SeqCup consistently outperforms the V method. For q_1, SeqCup achieves 89.7% ±1.0 versus 92.9% for the V method, but as the number of displaced points increases, the V method shows a significant drop in performance. For q_6, V's efficacy drops to only 9.5%, while SeqCup maintains a much stronger performance of 70.5% ±1.1, and SeqCupMod reaches 87.4% ±1.1, far outperforming the V method.

AICc: For q_1, q_2, and q_4, SeqCup consistently performs better than AICc. However, for q_6, AICc (80.5%) outperforms SeqCup (70.5% ±1.1). SeqCupMod, with 87.4% ±1.1, performs better than both SeqCup and AICc in this case.

4.2 Numerical Example 2: GCT and Univariate Approach

Here, we also evaluated SeqCup-Free against the univariate model proposed by Erdogan et al. (2021), which similarly relies on the analysis of differences between observations in two epochs, rather than coordinate differences, and also considers the principles of the model error approach. The authors compared their results with GCT, which is classically referred to as CDA (Conventional Deformation Analysis). Thus, we also evaluated the efficacy of SeqCup-Free using the results from both the Univariate and CDA approaches described by these authors. The MSR metric was applied. For this, we used the same network (Fig. 16) and the same simulation settings, as detailed in the original work by Erdogan et al. (2021). The magnitudes of the displacements were randomly selected from two intervals: [MDD, 2MDD] and [MDD, 3MDD], where MDD refers to the Minimal Detectable Displacement, with a value of 2.2 mm for this network. The first interval comprises 2.2 mm and 4.4 mm displacements, while the second covers 2.2 mm to 6.6 mm. In this experiment, we also considered the case where the false alarm rate $\mathcal{P}_{FA}$ was not controlled, ensuring comparability with the results of the authors mentioned above, who did not control for false alarms. Additionally, 50 trials with 10,000 Monte Carlo experiments were conducted to account for the uncertainty of the simulation process ($\pm\sigma_{MC}\%$), as in the previous evaluation. This process enabled comparison with the results found in the cited literature.

If we applied the stricter criterion for selecting the maximum number of points, given by $\min\left(\min r_{ll}\right)_{g_i}^{q_{\max}} > 0.5$, the network would be diagnosed as having low redundancy, with SeqCup-Free capacity limited to $q_{\max} = 1$. However, by applying the softer criterion $avg(\min r_{ll})_{g_i}^{q_{\max}} > 0.5$, according to Eq.(29), we would obtain $q_{\max} = 4$. We

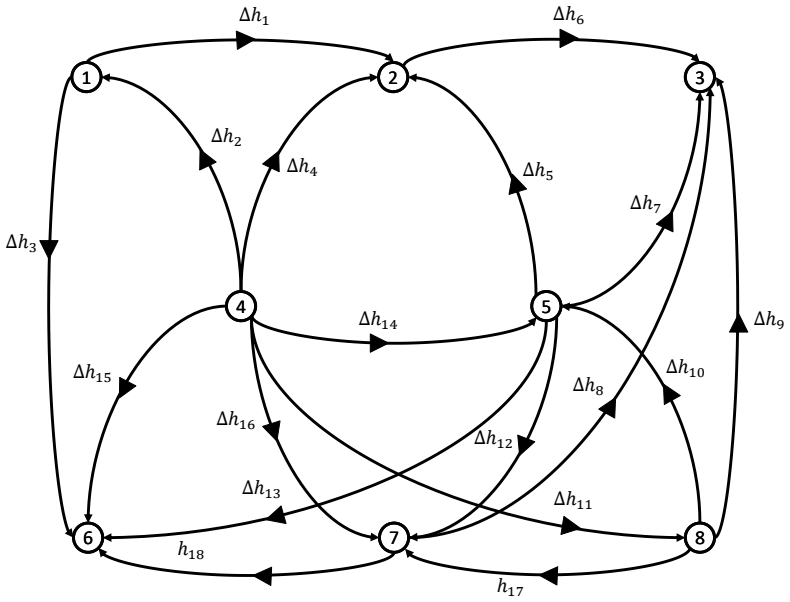

Fig. 16 Configuration of the leveling control network based on Erdogan et al. (2021)

employed the latter criterion to meet the simulation standards set by the authors mentioned above, who tested scenarios for each MDD interval, with one randomized displaced point (q_1), two randomized displaced points (q_2), and three randomized displaced points (q_3).

The $\mathcal{P}_{FA}$ for SeqCup-Free was set to $\alpha = 0.001$, $\alpha = 0.01$, and $\alpha = 0.05$, with their corresponding critical values $c_\alpha = 14.6809$, $c_\alpha = 10.3663$, and $c_\alpha = 7.3873$, obtained from the Monte Carlo approach in Appendix (B) for 2,000,000 Monte Carlo experiments (denoted by SeqCup in Tables 10 and 11). As mentioned previously, SeqCup-Free was also evaluated for the case where $\mathcal{P}_{FA}$ is not controlled (denoted by SeqCup$_{FA}$ in Tables 10 and 11). In the latter case, the critical values were computed from $\chi^2_{df=1,\alpha}$, where $df = q_1$, representing the degrees of freedom under the condition that one displaced point exists. The corresponding critical values for $\alpha = 0.001$, $\alpha = 0.01$, and $\alpha = 0.05$ are given by $c_\alpha = 10.8276$, $c_\alpha = 6.6349$, and $c_\alpha = 3.8415$, respectively.

The analysis of the results presented in Tables 10 and 11 reveals several important insights, especially when considering the number of displaced points q_j, the significance levels α, and the overall performance of the different methods (SeqCup, SeqCupMod, SeqCup$_{FA}$, Univariate Approach, and CDA).

In general, first, the impact of the number of displaced points q_j is clear throughout all methods. As the number of displaced points increases, the efficacy (MSR) of the correct model specification tends to decrease for all methods. This trend is particularly pronounced for q_3, where three points are displaced. Secondly, the significance levels (α) greatly affect the efficacy of the methods.

In the interval [MDD, 2MDD] (Table 10), for $\alpha = 0.001$, both SeqCup and SeqCupMod maintain relatively high efficacy for q_1 (71.6% and 71.7%, respectively), while the CDA and Univariate Approach methods show a sharp drop in efficacy (33.6% and 59.2%, respectively). This downward trend continues as q_j increases, with SeqCupMod demonstrating a slight advantage at q_2 and q_3.

Similarly, in the [MDD, 3MDD] interval (Table 11), the same pattern emerges. For $\alpha = 0.001$, SeqCup and SeqCupMod start with an efficacy of 85.5% for q_1, but this decreases to 50.2% and 55.2%, respectively, for q_3. The CDA method, in particular, shows an even greater reduction, achieving only 27.6% efficacy for q_3.

At $\alpha = 0.05$, SeqCup and SeqCupMod continue to outperform the other methods, particularly for q_1 and q_2, achieving more than 90% efficacy. However, SeqCup$_{FA}$, which does not control for false alarms, performs similarly well for q_3, with an efficacy of 84.9% in the [MDD, 3MDD] interval, highlighting the potential trade-off between false alarms and correct identification rates.

Third, when comparing the methods overall, SeqCup, SeqCupMod, and SeqCup$_{FA}$ consistently outperform the CDA and Univariate Approach methods. This trend is particularly noticeable as q_j increases.

SeqCup vs. SeqCupMod: Both methods show similar efficacy for q_1, but SeqCupMod tends to be more reliable as the number of displaced points increases. For q_3 in the [MDD, 3MDD] interval, SeqCupMod achieves 55.2%, whereas SeqCup reaches 50.2%.

SeqCup$_{FA}$: Without false alarm control, this method shows higher efficacy for q_3, particularly at $\alpha = 0.05$, where it reaches 84.9% in the [MDD, 3MDD] interval. This reflects the increased freedom in recognizing displacements, although at the potential cost of increased false positives.

CDA and Univariate Approach: These methods perform significantly worse, especially as q_j increases. The Univariate Approach relies on the estimation of the mean difference of observations between two epochs. As a result, the univariate approach experiences reduced redundancy, which reduces the success rate of identification.

In general, the SeqCup, SeqCupMod, and SeqCup$_{FA}$ methods consistently show superior efficacy across all significance levels and for different quantities of displaced points. SeqCup, in particular, is more effective in identifying multiple displaced points, making it a good option for networks with low redundancy and multiple displacements. However, as demonstrated by the results of the previously analyzed network, SeqCupMod proves to be the better option for networks with higher redundancy.

5 Contribution

The practical applicability of SeqCup-Free in simulated networks, such as trilateration and leveling networks, demonstrates the method's versatility. Its ability to perform well in both real and theoretical network setups highlights its performance across different geodetic monitoring configurations. Additionally, the combination of a sequential and combinatorial approach provides a more comprehensive and resilient solution compared to purely iterative or combinatorial methods. In addition,

Table 10 Efficacy (MSR) of the correct model specification for different methods for the interval [MDD, 2MDD] mm based on Erdogan et al. (2021) [%].

α	q_j	SeqCup	SeqCupMod	SeqCup^{FA}	Univariate Approach	CDA
0.001	0	99.9	99.9	99.2 ± 0.1	97.5	99.5
	1	71.6 ± 0.5	71.7 ± 0.5	82.0 ± 0.4	59.2	33.6
	2	45.8 ± 0.5	46.2 ± 0.5	63.0 ± 0.6	19.9	16.1
	3	19.9 ± 0.4	23.9 ± 0.4	37.3 ± 0.5	3.1	9.3
0.01	0	99.0	99.0	92.5	82.6	97.7
	1	83.1 ± 0.3	83.1 ± 0.3	86.5 ± 0.4	71.2	56.3
	2	65.5 ± 0.5	66.3 ± 0.5	78.2 ± 0.5	54.8	37.6
	3	40.0 ± 0.7	47.6 ± 0.7	60.2 ± 0.3	33.8	26.8
0.05	0	95.0	95.0	68.2	40.8	92.3
	1	86.8 ± 0.3	86.9 ± 0.3	69.8 ± 0.3	44.0	71.1
	2	76.5 ± 0.4	77.6 ± 0.4	70.2 ± 0.5	45.7	56.8
	3	56.0 ± 0.5	66.8 ± 0.5	71.6 ± 0.5	45.1	46.5

Table 11 Efficacy (MSR) of the correct model specification for different methods for the interval [MDD, 3MDD] mm based on Erdogan et al. (2021) [%].

α	q_j	SeqCup	SeqCupMod	SeqCup^{FA}	Univariate Approach	CDA
0.001	1	85.5 ± 0.3	85.5 ± 0.3	90.6 ± 0.3	76.5	58.6
	2	70.4 ± 0.4	70.6 ± 0.4	80.6 ± 0.3	42.5	39.2
	3	50.2 ± 0.7	55.2 ± 0.7	64.4 ± 0.3	11.7	27.6
0.01	1	90.8 ± 0.3	91.1 ± 0.3	89.9 ± 0.2	77.6	74.7
	2	81.9 ± 0.3	82.1 ± 0.3	86.3 ± 0.4	69.2	60.6
	3	65.7 ± 0.3	72.2 ± 0.3	78.7 ± 0.4	53.9	50.3
0.05	1	91.4 ± 0.3	91.3 ± 0.3	70.7 ± 0.4	45.4	81.1
	2	86.6 ± 0.3	86.9 ± 0.3	72.8 ± 0.5	49.4	73.0
	3	76.3 ± 0.4	83.2 ± 0.4	84.9 ± 0.3	52.5	65.9

the geometry-free approach, which utilizes differences in observations rather than adjusted coordinates, eliminates the need to define the network's datum. As a result, the method also avoids the loss of statistical power that typically accompanies the linearization of models.

The proposed methodology presents several noteworthy contributions. Firstly, the definition of the maximum number of points to be inspected as displaced is based on redundancy. Two metrics, derived from the criteria of minimum and mean of the smallest redundancies of possible displaced point combinations, prevent the issue of statistical overlap. It is worth mentioning that in all experiments, we observed no statistical overlap when adopting an appropriate $q_{\max}$. Although the choice between the two metrics may still appear subjective, we recommend the more rigorous criterion based on the minimum of the smallest redundancies. This approach ensures a higher level of reliability when identifying potentially displaced points within the network. This approach will be extended to outlier detection.

The efficient control of the Probability of False Alarm ($\mathcal{P}_{FA}$) through Monte Carlo simulations stands out as a substantial improvement over previous methods, which often lacked proper control of false positive rates. This ensures that the SeqCup-Free approach maintains a high level of reliability when applied to geodetic networks.

Here, we also applied a modified version of SeqCup, denoted by SeqCupMod. It introduces an innovative approach by adopting non-nested hypothesis tests. This eliminates the need to verify whether the null hypothesis is a subset of the alternative hypothesis, simplifying the process of identifying unstable points. The method's success rate, which surpasses previous approaches, suggests that SeqCupMod has significant potential for applications in network monitoring.

Despite these contributions, the method presents some limitations. Although SeqCupMod demonstrates higher success rates, its theoretical structure still requires further investigation to fully understand the reasons behind its enhanced performance when adopting non-nested hypothesis tests. More in-depth theoretical studies will help uncover the underlying mechanisms that contribute to these success rates.

Acknowledgements

This section will be completed after the acceptance of the manuscript.

Data availability

The datasets generated during and/or analysed during the current study are available from the corresponding author on reasonable request.

Conflict of interest

The authors declare that there is no conflict of interest.

Funding

This section will be completed after the acceptance of the manuscript.

Author contribution

This section will be completed after the acceptance of the manuscript.

Vinicius Francisco Rofatto - https://orcid.org/0000-0003-1453-7530
Marcelo Tomio Matsuoka - https://orcid.org/0000-0002-2630-522X
Lincon Rodrigues Silva - https://orcid.org/0009-0000-5951-4434
Ivandro Klein - https://orcid.org/0000-0003-4296-592X
Paulo de Oliveira Camargo - https://orcid.org/0000-0001-7648-1291
Mauricio Roberto Veronez - https://orcid.org/0000-0002-5914-3546
Luiz Gonzaga da Silveira Jr. - https://orcid.org/0000-0002-7661-2447.

Appendix A General Form of the Generalized Likelihood Ratio Tests

The probability density function (PDF) Φ_N under $\mathcal{H}_0$ is given by:

$$\Phi_N\left(\boldsymbol{\Delta e} \mid \mathcal{H}_0\right) = \exp\left\{-0.5\left[\left(\boldsymbol{\Delta e}-\mathbf{0}\right)^T \boldsymbol{\Sigma}_{\boldsymbol{\Delta e}}^{-1}\left(\boldsymbol{\Delta e}-\mathbf{0}\right)\right]\right\} \tag{A1}$$

For each alternative hypothesis $\mathcal{H}_{g_i}^{q_j}$, the corresponding PDFs are expressed as

$$\begin{aligned}\Phi_{N_i}\left(\boldsymbol{\Delta e} \mid \mathcal{H}_{g_i}^{q_j}\right) = \exp\left\{-0.5\left[\left(\boldsymbol{\Delta e}-\boldsymbol{C}_{g_i}^{q_j}\hat{\boldsymbol{\nabla}}_{g_i}^{q_j}\right)^T \boldsymbol{\Sigma}_{\boldsymbol{\Delta e}}^{-1}\left(\boldsymbol{\Delta e}-\boldsymbol{C}_{g_i}^{q_j}\hat{\boldsymbol{\nabla}}_{g_i}^{q_j}\right)\right]\right\}, \\ \text{for} \quad i=1,\ldots,K_{n_p}^{q_j}\end{aligned} \tag{A2}$$

The generalized likelihood ratio tests (GLRT) can be then computed (e.g., Teunissen (2006)) as follows:

$$\begin{aligned}T_{g_i}^{q_j} &= \frac{\max \Phi_N\left(\boldsymbol{\Delta e} \mid \mathcal{H}_0\right)}{\max \Phi_{N_i}\left(\boldsymbol{\Delta e} \mid \mathcal{H}_{g_i}^{q_j}\right)}, \\ &= \frac{\exp\left\{-0.5\left[\left(\boldsymbol{\Delta e_0}-\mathbf{0}\right)^T \boldsymbol{\Sigma}_{\boldsymbol{\Delta e}}^{-1}\left(\boldsymbol{\Delta e_0}-\mathbf{0}\right)\right]\right\}}{\exp\left\{-0.5\left[\left(\boldsymbol{\Delta e}-\boldsymbol{C}_{g_i}^{q_j}\hat{\boldsymbol{\nabla}}_{g_i}^{q_j}\right)^T \boldsymbol{\Sigma}_{\boldsymbol{\Delta e}}^{-1}\left(\boldsymbol{\Delta e}-\boldsymbol{C}_{g_i}^{q_j}\hat{\boldsymbol{\nabla}}_{g_i}^{q_j}\right)\right]\right\}}, \\ &= \underbrace{\left(\boldsymbol{\Delta e_0}\right)^T \boldsymbol{W}\left(\boldsymbol{\Delta e_0}\right)}_{\mathcal{H}_0} - \underbrace{\left(\boldsymbol{\Delta e}_{g_i}^{q_j}\right)^T \boldsymbol{W}\left(\boldsymbol{\Delta e}_{g_i}^{q_j}\right)}_{\mathcal{H}_A}, \quad i=1,\ldots,K_{n_p}^{q_j}\end{aligned} \tag{A3}$$

in which $\max \Phi_N\left(\boldsymbol{\Delta e} \mid \mathcal{H}_0\right)$ and $\max \Phi_{N_i}\left(\boldsymbol{\Delta e} \mid \mathcal{H}_{g_j}^{q_j}\right)$ are the maximum likelihood of the error vector $\boldsymbol{\Delta e}$ under $\mathcal{H}_0$ and under the alternative hypotheses $\mathcal{H}_{g_i}^{q_j}$, $i = 1,\ldots,K_{n_p}^{q_j}$, respectively. The constant term $(2\pi)^{-n/2}|\boldsymbol{\Sigma}_{\boldsymbol{\Delta e}}|^{-1/2}$ was omitted from the GLRT because it appears in the PDFs for both the null and alternative hypotheses. In this case, the test statistic of interest is the maximum value, given by:

$$T_{\max}^{q_j} = \max_{i \in 1,\ldots,K_{n_p}^{q_j}} T_{g_i}^{q_j}, \tag{A4}$$

Appendix B Monte Carlo Approach for Controlling the False Alarm Rate

When performing multiple hypotheses tests, there is the probability of committing at least one false discovery (false alarm), or Type I Error. Thus, the probability of a false alarm ($\mathcal{P}_{FA}$) for the case where SecUp-Free is in play corresponds to the probability of incorrectly detecting at least one point as displaced while in fact there is none (i.e., accept at least one alternative hypothesis when, in fact, the null hypothesis is true). This means that the $\mathcal{P}_{FA}$ for SecUp-Free does not depend on all subsequent

test steps, only on the extreme test statistic computed in its first step, i.e., only for $T^{q_1}_{\max}$. The risk of rejecting a true $\mathcal{H}_0$ is now one-fold: the undesired random event "reject a true $\mathcal{H}_0$" can occur in any of the $K^{q_1}_{n_p} = n_p$ tests. Let the probability of rejecting a true $\mathcal{H}_0$ in test 'k' be α_k (the so-called "experimentwise error rate") and let $\alpha_k << 1$. Furthermore, assume the random events "reject a true $\mathcal{H}_0$ in test 'k' to be approximately statistically independent. Then the total probability of rejecting a true $\mathcal{H}_0$ in the multiple hypothesis test (the so-called "familywise error rate", denoted here by α) is Lehmann and Lösler (2017):

$$\alpha \approx \sum_{k=1}^{n_p} \alpha_k \tag{B5}$$

The classical and well-known procedure to control the $\mathcal{P}_{FA}$ is to apply the Bonferroni equation by choosing Abdi (2007):

$$\alpha_k := \frac{\alpha}{n_p} \tag{B6}$$

Unfortunately, the test statistics $T^{q_1}_{g_1}$ and consequently the random events "reject a true $\mathcal{H}_0$ in test k are statistically dependent. The extreme statistic $T^{q_1}_{\max}$ captures such dependencies, as it is extracted from the $T^{q_1}_{g_k}$, $k = 1, \ldots, n_p$. If such dependencies are neglected, then the computed critical values are erroneous, and the test decisions do not have the user-defined family-wise error rate α. Here, the maximum test value $T^{q_1}_{\max}$ is treated directly as a test statistic. The decision rule is based on a one-sided test of the form $T^{q_1}_{\max} <= c_\alpha$. However, the distributions of $T^{q_1}_{\max}$ cannot be derived from well-known test distributions (e.g., χ^2-distribution). Therefore, critical values cannot be taken from a statistical table but should be computed numerically. A rigorous computation of critical values requires a Monte Carlo technique.

1. Generate a sequence of M random vectors of the measurement errors for both Epoch 1 $\boldsymbol{e_v}^{(1)}_m$ and Epoch 2 $\boldsymbol{e_v}^{(2)}_m$, $m = 1, \ldots, M$ of the desired distribution. e.g.:

$$\begin{cases} \boldsymbol{e_v}^{(1)}_m \sim N\left(\mathbf{0}, \boldsymbol{\Sigma_y}^{(1)}\right) & \text{for Epoch 1} \\ \boldsymbol{e_v}^{(2)}_m \sim N\left(\mathbf{0}, \boldsymbol{\Sigma_y}^{(2)}\right) & \text{for Epoch 2} \end{cases}, \quad m = 1, \ldots, M \tag{B7}$$

   where M is known as the number of Monte Carlo experiments. In addition, Matlab's 'mvnrnd' command may be used in this step, for example.
2. For each pair $\boldsymbol{e_v}^{(1)}_m$ and $\boldsymbol{e_v}^{(2)}_m$, $m = 1, \ldots, M$, compute the differences in errors between the two epochs, i.e.:

$$\boldsymbol{\Delta e}_m = \boldsymbol{e_v}^{(2)}_m - \boldsymbol{e_v}^{(1)}_m, \quad m = 1, \ldots, M \tag{B8}$$

3. Assemble the displacement-design matrix for q_1 such that $\left(\boldsymbol{C}^{q_1}_{g_i}\right)_m$, $i = 1, \ldots, n_p$, for each Monte Carlo experiment, $m = 1, \ldots, M$. If we have a trilateration network at hand, then the signs of the coefficients of the displacement-design matrix can be obtained according to sign function $\text{sign}(\boldsymbol{\Delta e}_m)$, $m = 1, \ldots, M$. Next, compute the

test statistic from Eq.(10) and then the maximum from Eq.(13) for each Monte Carlo experiment, i.e., $(T^{q_1}_{\max})_m$, $m = 1, \ldots, M$.

4. Sort in ascending order the $(T^{q_1}_{\max})_m$, getting a sorted vector $\boldsymbol{T_s}$, such that:

$$\boldsymbol{T_s} = (T^{q_1}_{\max})_1 < (T^{q_1}_{\max})_2 , \ldots , < (T^{q_1}_{\max})_M \tag{B9}$$

The sorted values in the vector $\boldsymbol{T_s}$ provide a discrete representation of the cumulative density function of the maximum test statistic $T^{q_1}_{\max}$.

5. Determine the critical value c_α (e.g., Lehmann (2012)):

$$c_\alpha = \frac{1}{2}\left(\boldsymbol{T_s}_{[(1-\alpha)M]} + \boldsymbol{T_s}_{[(1-\alpha)M]+1}\right) \tag{B10}$$

where [.] denotes rounding down to the next integer that indicates the position of the selected elements in the ascending order of $\boldsymbol{T_s}$. This position corresponds to a critical value for a stipulated $\mathcal{P}_{FA}$ (α). This can be done for a sequence of values α in parallel.

References

Abdi H. The Bonferroni and Sidák corrections for multiple comparisons. In: Salkind N, editor. Encyclopedia of Measurement and Statistics. Thousand Oaks, CA: Sage; 2007. .

Aydin C. Effects of Displaced Reference Points on Deformation Analysis. Journal of Surveying Engineering. 2017;143(3):04017001. https://ascelibrary.org/doi/abs/10.1061/%28ASCE%29SU.1943-5428.0000216, https://doi.org/10.1061/(ASCE)SU.1943-5428.0000216.

Baarda W. A testing procedure for use in geodetic networks. Publications on Geodesy, New Series. 1968;2(5). https://www.ncgeo.nl/index.php/en/publicatiesgb/publications-on-geodesy/item/2515-pog-09-w-baarda-a-testing-procedure-for-use-in-geodetic-networks, netherland Geodetic Commission, Delft, The Netherlands.

Baarda W. S-Transformation and Criterion Matrices. Publications on Geodesy, New Series. 1973;5(1). https://www.ncgeo.nl/index.php/en/publicatiesgb/publications-on-geodesy/item/2515-pog-09-w-baarda-a-testing-procedure-for-use-in-geodetic-networks, netherland Geodetic Commission, Delft, The Netherlands.

Baselga S. Exhaustive search procedure for multiple outlier detection. Acta Geodaetica et Geophysica Hungarica. 2011 Dec;46(4):401–416. https://doi.org/10.1556/AGeod.46.2011.4.3.

Batilović M, Đurović R, Sušić Z, Željko Kanović, Cekić Z. Robust Estimation of Deformation from Observation Differences Using Some Evolutionary Optimisation

Algorithms. Sensors. 2022;22(1):159. https://www.mdpi.com/1424-8220/22/1/159, https://doi.org/10.3390/s22010159.

Biagi L, Caldera S. An Efficient Leave One Block Out approach to identify outliers. Journal of Applied Geodesy. 2013;7(1):11–19. https://doi.org/doi:10.1515/jag-2012-0030.

Box GEP, Muller ME. A Note on the Generation of Random Normal Deviates. The Annals of Mathematical Statistics. 1958;29(2):610–611. https://doi:10.1214/aoms/1177706645.

Caspary WF. Concepts of network and deformation analysis. Rueger JM, editor, School of Geomatic Engineering, University of New South Wales; 2000.

Chen YQ. Analysis of deformation surveys—a generalized method. University of New Brunswick, Fredericton; 1983.

Duchnowski R. Median-Based Estimates and Their Application in Controlling Reference Mark Stability. Journal of Surveying Engineering. 2010;136(2):47–52. https://doi.org/10.1061/(ASCE)SU.1943-5428.0000014.

Duchnowski R. Hodges–Lehmann estimates in deformation analyses. Journal of Geodesy. 2013 Nov;87(10):873–884. https://doi.org/10.1007/s00190-013-0651-2.

Durdag UM, Hekimoglu S, Erdogan B. Reliability of Models in Kinematic Deformation Analysis. Journal of Surveying Engineering. 2018;144(3):04018004. https://doi.org/10.1061/(ASCE)SU.1943-5428.0000254.

Erdogan B, Hekimoglu S, Durdag UM. A new univariate deformation analysis approach considering displacements as model errors. Studia Geophysica et Geodaetica. 2021 Jan;65(1):1–14. https://doi.org/10.1007/s11200-020-1024-y, https://doi.org/10.1007/s11200-020-1024-y.

Hekimoglu S, Erdogan B, Soycan M, Durdag UM. Univariate Approach for Detecting Outliers in Geodetic Networks. Journal of Surveying Engineering. 2014;140(2).

Hekimoglu S, Erdogan D, Butterworth S. Increasing the Efficacy of the Conventional Deformation Analysis Methods: Alternative Strategy. Journal of Surveying Engineering. 2010;136(2):53–62.

Hekimoglu S, Koch KR. How can reliability of the robust methods be measured? In: Altan MO, Gründig L, editors. Third Turkish-German joint geodetic days, vol. 1 Istanbul Technical University, Istanbul, Turkey; 1999. p. 179–196.

Heunecke O, Kuhlmann H, Welsch WM, Eichhorn A, Neuner H. Handbuch Ingenieurgeodäsie: Auswertung geodätischer Überwachungsmessungen. 2 ed. Wichmann; 2013.

Klein I, Matsuoka MT, Guzatto MP, Nievinski FG. An approach to identify multiple outliers based on sequential likelihood ratio tests. Survey Review. 2017;49(357):449–457. https://doi.org/10.1080/00396265.2016.1212970.

Lehmann R. Improved critical values for extreme normalized and studentized residuals in Gauss–Markov models. Journal of Geodesy. 2012 Dec;86(12):1137–1146. https://doi.org/10.1007/s00190-012-0569-0, https://doi.org/10.1007/s00190-012-0569-0.

Lehmann R, Lösler M. Congruence analysis of geodetic networks – hypothesis tests versus model selection by information criteria. Journal of Applied Geodesy. 2017;11(4):271–283. https://doi.org/10.1515/jag-2016-0049.

Lehmann R, Lösler M. Hypothesis Testing in Non-Linear Models Exemplified by the Planar Coordinate Transformations. Journal of Geodetic Science. 2018;8(1):98–114. https://doi.org/10.1515/jogs-2018-0009, https://doi.org/doi:10.1515/jogs-2018-0009.

Matsumoto M, Nishimura T. Mersenne twister: A 623-dimensionally equidistributed uniform pseudo-random number generator. ACM Transactions on Modeling and Computer Simulation. 1998 Jan;8(1):3–30. https://dl.acm.org/citation.cfm?id=272991.

Mierlo JV. A Testing Procedure for Analysing Geodetic Deformation Measurements. In: In Proceedings of the II. International Symposium of Deformation Measurements by Geodetic Methods Bonn, Germany: Konrad Wittwer, Stuttgart; 1978. p. 79–103.

Mierlo JV. Statistical Analysis of Geodetic Measurements for the Investigation of Crustal Movements. In: Whitten CA, Green R, Meade BK, editors. Recent Crustal Movements, 1977 vol. 13 of Developments in Geotectonics. Elsevier; 1979. p. 457 – 467. http://www.sciencedirect.com/science/article/pii/B9780444417831500726. http://www.sciencedirect.com/science/article/pii/B9780444417831500726.

Niemeier W. Statistical Tests for Detecting Movements in Repeatedly Measured Geodetic Networks. In: VYSKOČIL P, GREEN R, MÄLZER H, editors. Recent Crustal Movements, 1979 vol. 16 of Developments in Geotectonics. Elsevier; 1981. p. 335–351. https://www.sciencedirect.com/science/article/pii/B9780444419538500414. https://www.sciencedirect.com/science/article/pii/B9780444419538500414.

Nowel K. Squared Msplit(q) S-transformation of control network deformations. Journal of Geodesy. 2019 Jul;93(7):1025–1044. https://doi.org/10.1007/s00190-018-1221-4, https://doi.org/10.1007/s00190-018-1221-4.

Nowel K. Specification of deformation congruence models using combinatorial iterative DIA testing procedure. Journal of Geodesy. 2020 Nov;94(12):118. https://doi.org/10.1007/s00190-020-01446-9, https://doi.org/10.1007/s00190-020-01446-9.

Nowel K, Kamiński W. Robust estimation of deformation from observation differences for free control networks. Journal of Geodesy. 2014 Aug;88(8):749–764. https://doi.org/10.1007/s00190-014-0719-7.

Pelzer H. Zur Analyse geodätischer Deformationsmessungen. PhD thesis, Deutsche Geodätische Kommission, Reihe C: Dissertationen - Heft Nr. 164, München, Germany; 1971.

Prószyński W, Kwaśniak M. Analytic tools for investigating the structure of network reliability measures with regard to observation correlations. Journal of Geodesy. 2018 Mar;92(3):321–332. https://doi.org/10.1007/s00190-017-1064-4, https://doi.org/10.1007/s00190-017-1064-4.

Rofatto VF, Matsuoka MT, Klein I, Veronez MR, Bonimani MLS, Lehmann R. A half-century of Baarda's concept of reliability: a review, new perspectives, and applications. Survey Review. 2020;52(372):261–277. https://doi.org/10.1080/00396265.2018.1548118.

Rofatto VF, Matsuoka MT, Klein I, Veronez MR, Silveira Jr LG. A Monte Carlo-Based Outlier Diagnosis Method for Sensitivity Analysis. Remote Sensing. 2020;12(5). https://www.mdpi.com/2072-4292/12/5/860, https://doi.org/10.3390/rs12050860.

Teunissen PJG. Distributional theory for the DIA method. Journal of Geodesy. 2018 Jan;92(1):59–80. https://doi.org/10.1007/s00190-017-1045-7.

Teunissen PJG. The geometry of geodetic inverse linear mapping and non-linear adjustment. Publications on Geodesy, New Series. 1985;8(1). Netherland Geodetic Commission, Delft, The Netherlands.

Teunissen PJG. Testing Theory: an introduction. 2 ed. Delft University Press; 2006.

Velsink H. Testing Methods for Adjustment Models with Constraints. Journal of Surveying Engineering. 2018;144(4). https://doi.org/10.1061/(ASCE)SU.1943-5428.0000260.

Velsink H. On the deformation analysis of point fields. Journal of Geodesy. 2015 Nov;89(11):1071–1087. https://doi.org/10.1007/s00190-015-0835-z.

Welsch WM, Heunecke O. Models and terminology for the analysis of geodetic monitoring observations. In: Official report of the ad-hoc committee of FIG working group 6.1: X FIG international symposium on deformation measurements. FIG - International Federation of Surveyors; 2001. https://www.fig.net/resources/publications/figpub/pub25/figpub25.asp. https://www.fig.net/resources/publications/figpub/pub25/figpub25.asp.

Wiśniewski Z, Zienkiewicz MH. Shift-Msplit* Estimation in Deformation Analyses. Journal of Surveying Engineering. 2016;142(4):04016015. https://doi.org/10.1061/(ASCE)SU.1943-5428.0000183.

Wujanz D, Avian M, Krueger D, Neitzel F. Identification of stable areas in unreferenced laser scans for automated geomorphometric monitoring. Earth Surface Dynamics. 2018;6(2):303–317.

Zienkiewicz MH. Application of Msplit estimation to determine control points displacements in networks with unstable reference system. Survey Review. 2015;47(342):174–180. https://doi.org/10.1179/1752270614Y.0000000105.

Zienkiewicz MH, Baryla R. Determination of vertical indicators of ground deformation in the old and main city of Gdansk area by applying unconventional method of robust estimation. Acta Geodynamica et Geomaterialia. 2015;12(3):249–257.

This preprint was submitted under the following conditions:

- The authors declare that they are aware that they are solely responsible for the content of the preprint and that the deposit in SciELO Preprints does not mean any commitment on the part of SciELO, except its preservation and dissemination.
- The authors declare that the necessary Terms of Free and Informed Consent of participants or patients in the research were obtained and are described in the manuscript, when applicable.
- The authors declare that the preparation of the manuscript followed the ethical norms of scientific communication.
- The authors declare that the data, applications, and other content underlying the manuscript are referenced.
- The deposited manuscript is in PDF format.
- The authors declare that the research that originated the manuscript followed good ethical practices and that the necessary approvals from research ethics committees, when applicable, are described in the manuscript.
- The authors declare that once a manuscript is posted on the SciELO Preprints server, it can only be taken down on request to the SciELO Preprints server Editorial Secretariat, who will post a retraction notice in its place.
- The authors agree that the approved manuscript will be made available under a Creative Commons CC-BY license.
- The submitting author declares that the contributions of all authors and conflict of interest statement are included explicitly and in specific sections of the manuscript.
- The authors declare that the manuscript was not deposited and/or previously made available on another preprint server or published by a journal.
- If the manuscript is being reviewed or being prepared for publishing but not yet published by a journal, the authors declare that they have received authorization from the journal to make this deposit.
- The submitting author declares that all authors of the manuscript agree with the submission to SciELO Preprints.